Multiphase Chemical Evolution in Elliptical Galaxies

Yutaka Fujita

Graduate School of Human and Environmental Studies,

Kyoto University, Kyoto 606-01, Japan

Yukawa Institute for Theoretical Physics,

Kyoto University, Kyoto 606-01, Japan

Junji Fukumoto

Cray Research Japan, Cuore Bldg., 9th Floor, 12-25, Hiroshiba-cho,

Suita-si, Osaka 564, Japan

Katsuya Okoshi

Department of Earth and Space Science,Faculty of Science,

Osaka University,Machikaneyama-cho, Toyonaka, Osaka 560, Japan

Received _____; accepted _____

ABSTRACT

The recent *ASCA* results show that the iron abundance of the X-ray gas of elliptical galaxies is less than the solar abundance ($Z_{\odot}$). The observed low iron abundance is inconsistent with the predictions of the previous chemical evolution models. In order to solve this problem, we present a simple model of chemical evolution for elliptical galaxies after the galactic wind period under the assumption that the gases ejected from stars do not mix with the circumferential gas. The ejected gas components evolve separately according to their birth time and origin. We have investigated their evolution qualitatively. The gas components originated from supernova remnant shells cool and drop out of the hot gas faster than the other components because of their high density and metal abundance. As a result, supernovae cannot heat the whole gas of the elliptical galaxies effectively, in contrary to the previous results. If the metal abundance of mass-loss gas is not uniform, the mass-loss gas with higher abundance also easily drops out and the average abundance can decrease. We believe that this is a hint of solving the low abundance problem.

Subject headings: galaxies : intergalactic medium - galaxies : interstellar matter - galaxies : X-rays

1. INTRODUCTION

It is now well established by X-ray observations that elliptical galaxies are often sources of thermal X-ray emission. Temperatures of the hot interstellar medium (ISM) are well-determined to be around 1 keV and X-ray luminosities are typically around 10^{40} erg. In contrast, until recently, we have had little information on the metal abundance and the spatial structure of the hot ISM due to the poor energy and spatial resolution of detectors. For this reason, in most of works on the chemical evolution for elliptical galaxies, it had been assumed that the gas ejected from stars spontaneously mixes with the ISM. This inevitably leads to the metal abundance of the ISM higher than the value for the sun, because the metal abundance of the stars in elliptical galaxies is higher than the value for the sun (e.g. Arimoto & Yoshii 1987 ; Matteucci & Tornambé 1987 ; Mihara & Takahara 1994 ; Matteucci & Gibson 1995 ; Fukumoto & Ikeuchi 1996).

The recent observations of *ASCA* (Awaki et al. 1994 ; Matsushita et al. 1994) have changed the situation of this problem significantly. The *ASCA* observations showed that the iron abundance of the hot ISM is less than that of the sun, which is inconsistent with the predictions of the previous simple chemical evolution models.

A hint of solving this problem is given by the recent *ROSAT* observation and theoretical argument. First, the recent *ROSAT* observation showed the inhomogeneity and the existence of cooling clumps in the hot ISM of NGC 507. (Kim & Fabbiano 1995) Second, Mathews (1990) indicated that the $\sim 1 M_{\odot}$ of metal ejected by each supernova event into the ISM is trapped locally within the hot bubbles and will never mix thoroughly with the ambient hot gas. He also argued that metal ejected through stellar wind may not mix either and make small fluctuation of metal abundance in the ISM. These observational and theoretical arguments suggest that the ISM is not well mixed, which is inconsistent with

the assumption of the previous chemical evolution models. If this is the case, we expect that gas components with higher metal abundance and density will cool faster than other components ; they go into cool phase and do not emit X-ray. This will reduce effectively the observed average abundance of the hot ISM. Renzini et al. (1993) has already explored the similar idea based on two-phase model and showed that the model does not reproduce the observed iron K line of NGC 1399, the cD galaxy in the Fornax cluster. Although the galaxies we investigated here are non-cD galaxies, we suggest that their two-phase model is too simple to explain the observation. In this paper, we investigate the chemical evolution of elliptical galaxies assuming that the gas released from stars does not mix with the ambient ISM ; we propose the multiphase model consisting of hundreds of gas phases and consider their evolutions.

The paper is organized as follows. First, in the next section we describe the fundamental assumptions in detail and write down the basic equations to determine the evolution of the iron abundance of the ISM. Then, in §3, we solve these equations numerically for some typical models. On the basis of this general analysis, in §4, we simulate the X-ray spectra of our model galaxies and discuss the possibility of accounting for the observed low iron abundance of the hot ISM by comparing these simulations with the observational data. Our conclusions are summarized in §5.

2. ASSUMPTION AND BASIC EQUATIONS

We consider the chemical evolution after galactic wind period. We assume for simplicity that an elliptical galaxy is a sphere of radius R and it is uniform on average, although it contains many gas components (hereafter called "phases"). The phases are classified by

their origin and birth time. We consider the three types of the origin, that is, gas ejected through stellar wind (mass-loss gas), shell and cavity of supernova remnants (SNRs). From now on, the phases of each type are called "mass-loss phase", "shell phase", and "cavity phase" indicated by the indices ML, s, and c, respectively. We divide time into a finite number of steps, $0 < t_0 < t_1 < ... < t_i < ... < t_n$, where t_0 and t_n are the start and end time of the calculation, respectively. We define $t = t_0 (= 0.5\mathrm{Gyr})$ as the time when the galactic wind stops. In each time-step, one phase is born for each type. The phase of type α (ML, s, or c) which is born in $t_{i-1} < t < t_i$ is called the (i, α)-th phase and has its own temperature $T^{(i,\alpha)}$, density $\rho^{(i,\alpha)}$, metal abundance $Z^{(i,\alpha)}$, and mass $M^{(i,\alpha)}$. Each phase radiates its thermal energy and evolves. We assume that energy transfer between the phases is worked only by pressure and ignore thermal conduction for simplicity. The phases are assumed to be in pressure equilibrium because sound crossing time of an elliptical galaxy is far shorter than its age (see Eq.(47)). Exceptionally, the phases whose temperatures become below $T_{\mathrm{crit}} (= 10^5\mathrm{K})$ are not considered to be in the pressure equilibrium because the condition of the pressure equilibrium will broken down for the phases due to the high cooling rate, although it also depends on size of each gas blob composing the phases (Cowie, Fabian, & Nulsen 1980). They are assumed to cool immediately and drop out of the hot ISM. This means that while the total number of the type of the phase is unchanged, the number of the phase whose temperature is above T_{crit} can be different among the types at the given time. The gas left after galactic wind is also considered as a phase called "zero-phase"or $(0, 0)$-th phase.

In §2.1, we describe the formation of the phases, and $t = t_i \, (1 \leq i \leq n)$ unless otherwise mentioned. In §2.2, we describe the evolution of the phases and the galaxy.

2.1. FORMATION OF EACH PHASE

2.1.1. Mass-Loss Phases

Here, we describe the formation of mass-loss phases. The relation between the mass of a star $m(\tau)$, and its lifetime τ, is given by

$$\log_{10} m(\tau) = 1.983 - 1.054\sqrt{\log_{10}\tau + 2.52}\,, \tag{1}$$

where the mass is in units of solar mass ($M_\odot$) and the lifetime is in units of Gyr. (Larson 1974). Because we consider the chemical evolution after galactic wind stops ($t > t_0 = 0.5$Gyr), this equation implies that we do not have to consider stars with mass larger than $2.85M_\odot$ in our calculation period. We assume that stars with mass in the range of $0.1 - 2.85M_\odot$ lose their masses by stellar winds ; we simply assume that the mass loss occurs instantaneously at the end of the life given by the fraction f of the initial mass of a star with m,

$$f = \begin{cases} 0 & \text{for } m \leq 0.7\,, \\ 0.42m & \text{for } 0.7 < m \leq 1.0\,, \\ 0.8 - 0.43/m & \text{for } 1.0 < m \leq 2.85\,, \end{cases} \tag{2}$$

(Köppen & Arimoto 1991). Further, we assume that the temperature of the gas ejected by the stellar wind immediately becomes equal to the virial temperature of the galaxy $\hat{T}$ for simplicity.

Under this assumption, the initial temperature and density of the mass-loss phase are then given by

$$T^{(i,ML)}(t_i) = \hat{T}\,, \tag{3}$$

$$\rho^{(i,ML)}(t_i) = \frac{\mu m_{\rm H} P(t_i)}{k_{\rm B}\hat{T}}\,, \tag{4}$$

where μ is the mean molecular weight ($= 0.6$), $m_{\rm H}$ is the mass of the hydrogen atom, $k_{\rm B}$ is Boltzmann constant, and $P(t)$ is the average pressure of the ISM. The pressure $P(t)$ is

obtained by solving the evolution equations of the galaxy described in §2.2.

The gas and iron mass of the mass-loss phase at its birth time, $M^{(i,ML)}(t_i)$ and $M_{\rm Fe}^{(i,ML)}(t_i)$, respectively, are given by

$$M^{(i,ML)}(t_i) = \int_{t_{i-1}}^{t_i} L_\star^{(ML)}(t)dt \,, \tag{5}$$

$$M_{\rm Fe}^{(i,ML)}(t_i) = \int_{t_{i-1}}^{t_i} L_{\rm Fe}^{(ML)}(t)dt \,, \tag{6}$$

where $L_\star^{(ML)}$ and $L_{\rm Fe}^{(ML)}$ are the gas and iron mass ejection rates from stars, respectively. Since the time scale of star formation in an elliptical galaxy, which is typically 10^{7-8} yr, is short enough compared with the galaxy age (e.g. Arimoto & Yoshii 1987), we assume that the stellar system of the galaxy formed at $t = 0$ simultaneously. Thus, $L_\star^{(ML)}$ and $L_{\rm Fe}^{(ML)}$ are given by

$$L_\star^{(ML)}(t) = f \left| \frac{dm(\tau)}{d\tau} \right|_{\tau=t} \phi(m(\tau = t)) M_\star(0) \,, \tag{7}$$

$$L_{\rm Fe}^{(ML)}(t) = Z_{\rm ML} f \left| \frac{dm(\tau)}{d\tau} \right|_{\tau=t} \phi(m(\tau = t)) M_\star(0) \,, \tag{8}$$

where $\phi(m)$, $M_\star(t)$ and $Z_{\rm ML}$ are the initial mass function (IMF), the stellar mass of the galaxy and the iron abundance of the mass-loss gas, respectively ; the power of the IMF is taken to be 1.35 and the other variables are given by later.

The density $\rho^{(i,ML)}(t_i)$, the temperature $T^{(i,ML)}(t_i)$, the mass $M^{(i,ML)}(t_i)$, and the iron mass $M_{\rm Fe}^{(i,ML)}(t_i)$ determined by above equations give the initial conditions of the evolution equations of the phases (see §2.2).

2.1.2. Shell and Cavity Phases

Next, we describe the formation of the shell and cavity phases. Since the progenitors of Type II supernovae have short lives $\tau < t_0$, Type II supernovae are important only in the

galactic wind period (e.g. Arimoto & Yoshii 1987 ; Matteucci & Tornambé 1987 ; David, Forman, & Jones 1991 ; Matteucci & Gibson 1995). Therefore, we consider only Type Ia supernovae (SN Ia) because we are concerned with chemical evolution after galactic wind stops.

We use the adiabatic Sedov solution in pressure equilibrium to determine the initial conditions of the shell and cavity phases for simplicity. The actual shape of the SNRs is deviated from the Sedov solution because of the high temperature of the unshocked gas. However, we confirmed that the deviation is not important (see §3).

For simplicity, we assume that the SNRs are consists of two parts, outer shell and inner cavity region, and that they evolve as separate phases. We call the former "shell phase" and the latter "cavity phase", denoted by the indices s and c, respectively. When the distance from the center of the SNR is r and the shock front radius is $r_{\rm s}$, the inner cavity region and the outer shell region correspond to $r < (1-k)r_{\rm s}$ and $(1-k)r_{\rm s} < r < r_{\rm s}$, respectively, where k is representing the width of the shell. In each region, the average density and temperature are decided as follows.

The shock front radius is given by

$$r_{\rm s} = \left(\frac{2.02 E_{\rm SN} t_{\rm s}^2}{\rho}\right)^{1/5} \tag{9}$$

(Spitzer 1978), where $E_{SN}(= 10^{51}{\rm erg})$ is the energy released from a supernova, t_s is the time past since the supernova explosion, and ρ is the average density of the ISM. The pressure just inside the shock front is given by

$$P_1 = \frac{2\rho}{(\gamma+1)}\left(\frac{dr_{\rm s}}{dt_{\rm s}}\right)^2 = \frac{8\rho^{3/5}(2.02E_{\rm SN})^{2/5}t_s^{-6/5}}{25(\gamma+1)} \tag{10}$$

(Spitzer 1978), where $\gamma(= 5/3)$ is the adiabatic constant.

We assume that P_1 is equal to the average pressure of the ISM P. Under the

assumption, the time $t_{\rm s}$ is given by

$$t_s = \left[\frac{8}{25(\gamma+1)}\right]^{5/6} P^{-5/6}(2.02E_{\rm SN})^{1/3}\rho^{1/2}\ , \tag{11}$$

and

$$r_{\rm s} = \left[\frac{8}{25(\gamma+1)}\right]^{1/3} P^{-1/3}(2.02E_{\rm SN})^{1/3}\ . \tag{12}$$

The density and pressure distribution of the Sedov solution, $\rho_{\rm Sedov}(r)$ and $P_{\rm Sedov}(r)$, respectively, are determined uniquely under the condition $P = P_1$.

In terms of r_s and $\rho_{\rm Sedov}(r)$, the average density in the shell region is expressed by

$$\rho_s = \int_{(1-k)r_{\rm s}}^{r_{\rm s}} 4\pi\rho_{\rm Sedov}(r)r^2dr \Big/ \int_{(1-k)r_{\rm s}}^{r_{\rm s}} 4\pi r^2dr\ . \tag{13}$$

The mass inside the shock front is given by

$$m_{\rm SNR} = \frac{4}{3}\pi r_{\rm s}^3\rho + m_{\rm pro}\ , \tag{14}$$

where $m_{\rm pro}$ is the mass of the progenitor star. The mass in the shell region is given by

$$m_{\rm s} = \rho_{\rm s}\int_{(1-k)r_{\rm s}}^{r_{\rm s}} 4\pi r^2dr\ . \tag{15}$$

Hence, the mass and average density in the cavity region are given by

$$m_{\rm c} = m_{\rm SNR} - m_{\rm s}\ , \tag{16}$$

$$\rho_{\rm c} = \frac{3m_{\rm c}}{4\pi(1-k)^3r_{\rm s}^3}\ . \tag{17}$$

The iron abundance is assumed to be uniform inside the shock front radius $r_{\rm s}$, because Mathews (1990) estimated that in an elliptical galaxy iron fragments made by Rayleigh - Taylor instability reach the shock front $\sim 10^4$ yr after the supernova explosion. The iron mass in the cavity and shell region are

$$m_{\rm Fe,s} = m_{\rm c}\left(\frac{m_{\rm Fe}}{m_{\rm SNR}} + \hat{Z}\right)\ , \tag{18}$$

$$m_{\rm Fe,c} = m_{\rm s}\left(\frac{m_{\rm Fe}}{m_{\rm SNR}} + \hat{Z}\right) , \tag{19}$$

where $m_{\rm Fe}$ is the iron mass ejected by the supernova and $\hat{Z}$ is the average iron abundance of the ISM occupied by the SNR.

Next, we determine the temperatures. For the Sedov solution, the specific thermal energy in the shell region is given by

$$U_s = \frac{1}{m_{\rm s}}\int_{(1-k)r_{\rm s}}^{r_{\rm s}} \frac{P_{\rm Sedov}}{\gamma - 1} 4\pi r^2 dr . \tag{20}$$

The specific thermal energy in the cavity region is given by

$$U_{\rm c} = (E_{\rm SN} - m_{\rm s}U_{\rm s})/m_{\rm c} . \tag{21}$$

Since the thermal energy of the ISM occupied by the SNR cannot be ignored, the average temperatures of the shell and cavity region are given by

$$T_{\rm s} = \frac{2}{3}\frac{\mu m_{\rm H} U_{\rm s}}{k_{\rm B}} + \hat{T} , \tag{22}$$

$$T_{\rm c} = \frac{2}{3}\frac{\mu m_{\rm H} U_{\rm c}}{k_{\rm B}} + \hat{T} , \tag{23}$$

respectively, where $\hat{T}(= P\mu m_{\rm H}/k_{\rm B}\rho)$ is the average temperature of the ISM which is assumed to be equals to the virial temperature. The densities and temperatures determined so far are adopted as the initial values of the shell and cavity phase for the evolution equations of the phases described in §2.2 as follows :

$$\rho^{(i,s)}(t_i) = \rho_s , \tag{24}$$

$$T^{(i,s)}(t_i) = T_s , \tag{25}$$

$$\rho^{(i,c)}(t_i) = \rho_c , \tag{26}$$

$$T^{(i,c)}(t_i) = T_c . \tag{27}$$

From Eqs. (12) - (23), they are determined uniquely if $E_{\rm SN}$, $m_{\rm pro}$, $m_{\rm Fe}$, k, ρ, $\hat{T}$, and $\hat{Z}$ are given. We fix $E_{\rm SN}$, $m_{\rm pro}$, and $m_{\rm Fe}$ by giving typical values, that is, $m_{\rm pro} = 2.0 M_\odot$, $m_{\rm Fe} = 0.75 {\rm M}_\odot$, and $E_{\rm SN} = 10^{51}$ erg. We also fix $k = 0.3$; the results in §3 are qualitatively unchanged even if we take the different value for $0.25 \lesssim k \lesssim 0.45$. The other parameters, ρ, $\hat{T}$, and $\hat{Z}$ are time-dependent and determined by solving the evolution equations of the galaxy described in §2.2. For examples, for $\rho = 1.67 \times 10^{-27}$g cm^{-3}, $\hat{T} = 1.3$ keV, and $\hat{Z} = 1.0 {\rm Z}_\odot$, we can estimate each quantity : $\rho_s = 2.4 \times 10^{-27}$g cm^{-3}, $\rho_c = 2.3 \times 10^{-28}$g cm^{-3}, $T_s = 1.8$ keV, $T_c = 9.6$ keV, and $m_{\rm Fe,s}/m_s = m_{\rm Fe,c}/m_c = 2.8 {\rm Z}_\odot$. Note that since the cooling function is nearly independent of temperature and inversely proportional to metal abundance near $T \sim 10^7$K (see Eq.(37)), the cooling time is proportional to $T/(\rho Z)$. Thus, the cooling time of the shell phase ($\propto T_s/(\rho_s m_{\rm Fe,s}/m_s)$) is generally shorter than that of the ambient medium ($\propto \hat{T}/(\rho \hat{Z})$). It causes selective cooling of the shell phase. This effect will be discussed in §3.

The gas and iron mass of the shell and cavity phase at their birth time are given by

$$M^{(i,s)}(t_i) = \int_{t_{i-1}}^{t_i} L_\star^{(s)}(t) dt \,, \tag{28}$$

$$M^{(i,c)}(t_i) = \int_{t_{i-1}}^{t_i} L_\star^{(c)}(t) dt \,, \tag{29}$$

$$M_{\rm Fe}^{(i,s)}(t_i) = \int_{t_{i-1}}^{t_i} L_{\rm Fe}^{(s)}(t) dt \,, \tag{30}$$

$$M_{\rm Fe}^{(i,c)}(t_i) = \int_{t_{i-1}}^{t_i} L_{\rm Fe}^{(c)}(t) dt \,, \tag{31}$$

where $L_\star^{(s)}$, $L_\star^{(c)}$, $L_{\rm Fe}^{(s)}$, and $L_{\rm Fe}^{(c)}$ are the mass and iron production rates of the shell and cavity phase, respectively ; they are given by

$$L_\star^{(s)}(t) = r_{\rm SN}(t) m_{\rm s}(t) \,, \tag{32}$$

$$L_\star^{(c)}(t) = r_{\rm SN}(t) m_{\rm c}(t) \,, \tag{33}$$

$$L_{\rm Fe}^{(s)}(t) = r_{\rm SN}(t) m_{\rm Fe,s}(t) \,, \tag{34}$$

$$L_{\rm Fe}^{(c)}(t) = r_{\rm SN}(t) m_{\rm Fe,c}(t) \,, \tag{35}$$

where $r_{\rm SN}(t)$ is the SN Ia rate. The time dependence of the SN Ia rate is assumed to be $r_{\rm SN}(t) \propto t^{-0.5}$ (David, Forman, & Jones 1990). The normalization is given by the SN Ia rate at $t = t_n$, which is specified later.

2.2. EVOLUTION OF THE PHASES AND THE GALAXY

The energy equation for the (i,α)-th phase for $t > t_i$ is given by

$$\frac{\rho^{(i,\alpha)}(t)}{\gamma - 1} \frac{d}{dt} \left(\frac{k_{\rm B} T^{(i,\alpha)}(t)}{\mu m_{\rm H}} \right) - \frac{k_{\rm B} T^{(i,\alpha)}(t)}{\mu m_{\rm H}} \frac{d}{dt} \rho^{(i,\alpha)}(t) = -(n_e^{(i,\alpha)})^2 \Lambda(Z^{(i,\alpha)}, T^{(i,\alpha)}(t)) \,, \tag{36}$$

where $n_e^{(i,\alpha)}$ is the electron density of the (i,α)-th phase and Λ is the cooling function. Assuming that the relative metal abundance is the same as that of the sun for simplicity, the cooling function is approximated by

$$\begin{aligned} \Lambda(Z^{(i,\alpha)}, T^{(i,\alpha)}) &= \left[2.1 \times 10^{-27} \left(1 + 0.1 \frac{Z^{(i,\alpha)}}{\rm Z_\odot} \right) \left(\frac{T^{(i,\alpha)}}{\rm K} \right)^{0.5} \right. \\ &+ \left. \left(0.04 + \frac{Z^{(i,\alpha)}}{\rm Z_\odot} \right) 6.2 \times 10^{-19} \left(\frac{T^{(i,\alpha)}}{\rm K} \right)^{-0.6} \right] \\ &\quad ({\rm ergs\,cm^{-3} s^{-1}}) \,. \end{aligned} \tag{37}$$

This is an empirical formula derived by fitting to the cooling curves in Figure 9-9 of Binney & Tremaine (1987).

In our model, all existing phases are assumed to be in pressure equilibrium because sound crossing time of an elliptical galaxy is far shorter than its age (see Eq.(47)). Thus, for $i < j$,

$$\rho(t_j) \frac{k_{\rm B} \hat{T}}{\mu m_{\rm H}} = \rho^{(i,\alpha)}(t_j) \frac{k_{\rm B} T^{(i,\alpha)}(t_j)}{\mu m_{\rm H}} = P(t_j) \,, \tag{38}$$

$$\rho(t_j) = \frac{M_{\rm g}(t_j)}{V(t_j)}\,, \tag{39}$$

where $M_{\rm g}$ and V are the total gas mass and volume of the galaxy, respectively. Here, we have approximated dP/dR by P/R for simplicity. Note that $V = (4\pi/3)R^3$.

The total gas mass, the iron mass and the gas volume are the summation of those of each phase ;

$$M_{\rm g}(t) = \sum_{\alpha} \sum_{i,\, T^{(i,\alpha)} > T_{\rm crit}} M^{(i,\alpha)}(t), \tag{40}$$

$$M_{\rm Fe}(t) = \sum_{\alpha} \sum_{i,\, T^{(i,\alpha)} > T_{\rm crit}} M_{\rm Fe}^{(i,\alpha)}(t), \tag{41}$$

$$V(t) = \sum_{\alpha} \sum_{i,\, T^{(i,\alpha)} > T_{\rm crit}} V^{(i,\alpha)}(t), \tag{42}$$

where

$$V^{(i,\alpha)}(t) = M^{(i,\alpha)}(t)/\rho^{(i,\alpha)}(t)\,. \tag{43}$$

As mentioned above, the phases whose temperatures are below $T_{\rm crit}(= 10^5{\rm K})$ are not included in the summation.

Note that part of the SNRs is composed of pre-existing phases. As mentioned in §2.1.2, we assumed that the SNRs evolve as new phases, then the masses of the pre-existing phases are reduced by the occupation by the SNRs. Thus, the mass and iron mass of the pre-existing (i,α)-th phase at $t = t_j$ $(i < j)$ are given by

$$M^{(i,\alpha)}(t_j) = M^{(i,\alpha)}(t_{j-1}) - M_{\rm SNR}^{(j)} \frac{V^{(i,\alpha)}(t)}{V(t)}\bigg|_{t=t_{j-1}}\,, \tag{44}$$

$$M_{\rm Fe}^{(i,\alpha)}(t_j) = M_{\rm Fe}^{(i,\alpha)}(t_{j-1}) - M_{\rm SNR}^{(j)} \frac{M_{\rm Fe}^{(i,\alpha)}(t)}{M^{(i,\alpha)}(t)} \frac{V^{(i,\alpha)}(t)}{V(t)}\bigg|_{t=t_{j-1}}\,, \tag{45}$$

respectively, where $M_{\rm SNR}^{(j)}$ is the mass occupied by SNRs during $t_{j-1} < t < t_j$, which is given by

$$M_{\rm SNR}^{(j)} = \int_{t_{j-1}}^{t_j} \frac{4}{3}\pi\rho(t) r_s(t)^3 r_{\rm SN}(t) dt\,. \tag{46}$$

We take the sound crossing time as the time-steps for the calculations,

$$t_{j+1} - t_j = \frac{R(t_j)}{\sqrt{GM(R(t_j))/R(t_j)}} = 4.7 \times 10^7 \mathrm{yr} \left(\frac{R}{10\mathrm{kpc}}\right)^{3/2} \left(\frac{M(R)}{10^{11}\mathrm{M}_\odot}\right)^{-1/2} . \quad (47)$$

Strictly speaking, calculations under Eq.(47) are not exact because the phases whose cooling time is shorter than the time-step are not treated correctly ; these phases are removed at the next time-step t_{j+1} and their PdV work in $t_j < t < t_{j+1}$ is not taken into account. However, we confirmed that in our examined models their PdV work is less than 10% of the variation of the total thermal energy of the galaxy in $t_j < t < t_{j+1}$. Then, we believe that it is negligible for our qualitative discussion.

We derive $\rho^{(i,\alpha)}(t_j)$ and $T^{(i,\alpha)}(t_j)$ from $\rho^{(i,\alpha)}(t_{j-1})$ and $T^{(i,\alpha)}(t_{j-1})$ by iterating Eqs.(36), (38), (39), (40), (42), and (44) until they converge.

3. NUMERICAL ANALYSIS

The main purpose of this section is to look into the qualitative features of the multiphase model of the hot ISM of the elliptical galaxy. We reduce the number of the free parameters by giving typical fixed values to some of them. First, for the parameters regarding the whole galaxy, we take $t_0 = 0.5$ Gyr, $t_\mathrm{n} = 10$ Gyr, $R(t_0) = 50$ kpc, $M_\star(0) = 2 \times 10^{11} M_\odot$, and $M_{\mathrm{g,Fe}}(t_0)/M_\mathrm{g}(t_0) = 4\mathrm{Z}_\odot$. We leave $M_\mathrm{g}(t_0)$ as a free parameter. Then if we specify $M_\mathrm{g}(t_0)$, we can write $V(t_0)^{(0,0)} = (4\pi/3)R(t_0)^3$, $M^{(0,0)}(t_0) = M_\mathrm{g}(t_0)$, and $M_\mathrm{Fe}^{(0,0)}(t_0) = M_{\mathrm{Fe,g}}(t_0)$. We take the temperature of the zero-phase $T^{(0,0)}(t_0) = 1.3$ keV. The virial temperature of the galaxy is given by

$$\hat{T} = T^{(0,0)}(t_0) \, (= 1.3\mathrm{keV}) \, . \quad (48)$$

Here, we discuss the validity of adopting the Sedov solution as the initial conditions of

the shell and cavity phases by comparison with the numerical simulation of evolution of a SNR in an elliptical galaxy. Mathews (1990) calculated the evolution of a SNR expanding into ISM with temperature $\hat{T} = 10^7$ K and density $\hat{n} = 10^{-3}\mathrm{cm}^{-3}$ until the pressure equilibrium is achieved. Figures 3 and 4 in his paper depict temperature and pressure distributions when the pressure equilibrium is almost achieved ($t_s = 1.17 \times 10^5$ yr). From now on, we call these the "Mathews solutions". Although Mathews showed the variations of temperature and pressure with radius only in the case of $\hat{T} = 10^7$ K and $\hat{n} = 10^{-3}\mathrm{cm}^{-3}$, the fact that the radius where the gas temperature has risen by ~ 2 above the ambient value ($\hat{T} = 10^7$ K) varies as $\hat{n}^{-1/3}$ (his Table 5) may indicate that the solution is self-similar ; we assume the self-similarity in the following argument. In the Mathews solution, the temperature and pressure gradients of the SNR are somewhat smaller than those of the Sedov solution. Thus, to obtain the similar values of ρ_s, ρ_c, T_s, and T_c, the shell width k must be larger when the Mathews solution is used in Eqs. (13) and (20) than that when the Sedov solution is used. For example, when $\hat{T} = 10^7$ K and $\hat{n} = 10^{-3}\mathrm{cm}^{-3}$, the values of ρ_s, ρ_c, T_s and T_c derived by using the Mathews solution and taking $k = 0.35$ are equal within 30% errors to those derived by using the Sedov solution and taking $k = 0.3$. We confirmed that the variation of 30% does not affect the results in this section significantly. Moreover, we confirmed that the results in this section are not significantly changed even if we use the Mathews solution and take $k = 0.3$.

We solve the basic equations described in §2 for the models whose details are given in Table 1. The difference between the models A and B is the initial gas mass $M_{\mathrm{g}}(t_0)$, which is chosen to match the observed X-ray luminosities of elliptical galaxies ($\sim 10^{40}\mathrm{erg\,s}^{-1}$) at $t = t_n$ (Table 2). Models A1 - A3 and B1 - B3 are calculated to see the effect of SN Ia. The SN Ia rate is normalized by the values at $t = t_n (= 10\mathrm{Gyr})$ shown in the third column of Table 1. The values are expressed in units of SNu, that is, the number of SNe per $10^{10}h^{-2}\mathrm{L}_{\mathrm{B}\odot}$ per 100 yr ($H_0 = 100h\mathrm{km\,s}^{-1}\,\mathrm{Mpc}^{-1}$; we set h=0.5). The ratio of the mass to

luminosity is taken to be $8M_\odot/L_\odot$, and the rate for SN Ia is normalized by using this ratio. Models A4 - A5 and B4 - B5 are calculated to see the effect of metal-abundance distribution for the mass-loss gas. In these models, the mass-loss phase born in each time-step is divided into two phases with equal masses and different abundances corresponding to the two figures for $Z_{\rm ML}$ (Table 1). On the other hand, in models A1 - A3 and B1 - B3, each component has the same abundance or the mass-loss gas has one kind of the abundance. Table 1 also shows total number of the time-step n and the numbers of phases which have survived (their temperature is above $T_{\rm crit}$) until $t = t_n$. In models B1 - B3, all phases cool and vanish by sometime before $t = t_n$, and we stopped the calculations at that time. We give the numbers of the survived phases in columns $N_{\rm ML,H}$, $N_{\rm ML,L}$, $N_{\rm sh}$, and $N_{\rm cav}$ denoting respectively the mass-loss phase with the high and low abundance, shell phase, and cavity phase (Table 1). Figures 1 - 4 show the time evolution of R, $M_{\rm g}$, and iron abundance Z, where Z represents $M_{\rm g,Fe}/M_{\rm g}$ in units of the solar abundance $\rm Z_\odot$, 1.7×10^{-3}.

Figures 1 and 2 show the influence of SN Ia on the gas evolution. The sharp decreases at $t \sim 4$ Gyr in Figure 1 and at $t \sim 3$ Gyr in Figure 2 represent cooling and vanishing of the zero-phase. Since the initial volume in series A is the same as in series B, the initial gas density is higher in series B than that in series A. Therefore, the cooling process is more effective and R decreases faster in series B than in series A. The radius of the gas sphere does not significantly increase even if the SN Ia rate at $t = t_n$ increases (Fig.1a and 2a). Furthermore, the gas mass decrease faster in the models of higher SN Ia rate (Fig.1b and 2b). These facts indicate that supernovae are not effective heating sources of the ISM as a whole. The reason is that the shell phases cool and drop out faster than other phases owing to their high density and metal abundance (see §2.1.2), and that they have large thermal energies when they are born as the following arguments shows. When a SNR becomes in

pressure equilibrium, the thermal energy within a shell region is given by

$$E_s = \frac{m_s T_s}{m_s T_s + m_c T_c} \left(E_{\rm SN} + \frac{2\pi k \hat{T}}{\mu m_{\rm H}} r_s^3 \rho \right) . \tag{49}$$

Since $E_s \gtrsim E_{\rm SN}$ in our parameter range, more energy than that supplied by supernova explosion is radiated from the shell region in a short time. Thus, supernovae cannot heat the ISM. This is contrary to the previous results (e.g. Ciotti et al. 1991 ; David et al. 1991) which claimed that supernovae are effective as heating sources and swell the ISM. However, *this fact does not reject the galactic wind model.* While the expanding SNRs do not overlap in our calculations, it is expected that they overlap during the galaxy-formation period because of the high supernova rate ; then, the ISM is expelled and galactic wind occurs (Ikeuchi 1977). Note that Mathews (1990) indicated the possibility of buoyant mixing of the hot cavity region in the local ISM. This may decrease entropy fluctuation and the effect of selective cooling of the shell phases.

In models A1, A2, B1, and B2, Z is around $\mathrm{Z}_\odot$ for $t \gtrsim 4$ Gyr (Fig.1c and 2c), because most of the mass of the remaining gas is dominated by mass-loss phases ($Z = 1\mathrm{Z}_\odot$). In models A3 and B3, the shell phases are dominant in mass ; they start to vanish for $t \gtrsim 6$ in model A3, and for $t \gtrsim 4$ in model B3.

As seen in Figures 3(c) and 4(c), Z is small when the mass-loss gas has two kinds of the iron abundance. This is because the mass-loss phases with the higher iron abundance also drop out in addition to the shell phases, as shown in Table 1. In models A4, A5, B4, and B5, $Z < \mathrm{Z}_\odot$ at $t = 10^{10}$ yr, which is consistent with the observations (Awaki et al. 1994 ; Matsushita et al. 1994). Although our model may be too simple to give quantitative predictions, we believe this is a hint of solving the low abundance problem of elliptical galaxies.

4. SPECTRAL SIMULATIONS

In most of observations, X-ray spectra of galaxies are fitted to at most two thin thermal plasma models. However, if the actual ISM is composed of many components with various temperatures and metal abundances, this simple fitting may give deferent values from the actual ones. In this section, we examine this possibility by constructing composite spectra from the many phases which have survived at $t = t_n$(=10 Gyr) and fit them to a few spectral models by the XSPEC package (ver. 8.50) as most of observers did, although our model may be too simple for detailed discussion.

We examine models A1, A2, and B4 because in the other models X-ray flux is below the observational limit (Table 2). The distance to the model galaxies is assumed to be 15 Mpc. In our models, several hundred phases are survived until the present epoch. However, the XSPEC package cannot treat so many phases ; for each type we collect each 10 phases into a new single phase. We regard the luminosity-weighted temperature and abundance of the 10 phases as the temperature and abundance of the new single phase. We confirmed that even if we collect each 20 phases into a new single phase, the results do not change significantly. First, the spectrum of each new phase is calculated by a thin thermal plasma model (so-called Meka model ; Mewe, Gronenschild, and van den Oord 1985 ; Mewe, Lemen, and van den Oord 1986 ; Kaastra 1992) in the XSPEC package. The reason of using Meka model is that the XSPEC package can treat high-abundance components only with this model. Then, using the XSPEC package, the spectral components are composed and the Galactic absorption ($10^{21}\mathrm{cm}^{-2}$) is taken into account. Since the cosmic iron abundance to which we referred as the solar abundance is 2.6×10^{-3} in the XSPEC package, we corrected it to 1.7×10^{-3} at composition. The model spectra are fitted to the Meka model plus an absorption with a response function of *ASCA* SIS. Background is not considered.

The exposure time and the results are shown in Table 2 ; the fluxes do not include absorption. For models A1, A2, and B4, the upper lines are the results of the fitting to one Meka model and the lower lines are those to two Meka models. For comparison, Z at $t = t_n (= 10$ Gyr) is also shown. The abundance $Z_{\rm ML}$, temperature $T_{\rm fit}$, and absorption column density $N_{\rm H,fit}$ derived by the fitting are also shown in Table 2. As clearly seen in Table 2, $Z_{\rm fit}$ is much smaller than Z when the model spectra are fitted to one Meka model plus absorption. However χ^2 is so large that these models will be rejected ; the fits suffer from significant positive residuals above ~ 2 keV as exemplified in Figure 5. We next fitted the spectra with a sum of two Meka models with different temperatures and normalizations but using common abundance as Matsushita et al. (1994) did. In these cases, χ^2 is significantly reduced. The fitted spectra are shown in Figure 6. All the models examined here are acceptable and the low abundance, $Z_{\rm fit} < Z_\odot$, is consistent with the observations (Awaki et al. 1994 ; Matsushita et al. 1994). The derived abundance $Z_{\rm fit}$ is still smaller than Z. This may indicate that not only χ^2 statics but also estimation of equivalent width of the lines is required to derive the metal abundance of multiphase gas (Matsushita, private communication). The iron K line is very weak (Figures 5 and 6), because of the small number of the survived shell phases (Table 2), and of the low density and high temperature (~ 10 keV) of the cavity phases. The weak iron K line is consistent with the observations (Awaki et al. 1994 ; Matsushita et al. 1994).

5. SUMMARY AND CONCLUSIONS

In this paper, we have presented a model of the chemical evolution for elliptical galaxies after galactic wind period under the assumption that the gases ejected from stars do not mix with the circumferential gas. The ejected gases evolve separately according to their

birth time and origin. We considered three origin of the ejected gas, that is, shell and cavity of supernova remnants and mass-loss. We fitted the model spectra made from the survived phases by thin thermal plasma models.

The main results and conclusions can be summarized as follows:

(i) The model predicts that the supernovae are not effective as heating sources of the ISM after the galactic wind stops. The shells of the supernova remnant can cool and drop out rapidly because of their high density and metal abundance. Since the shells initially have large thermal energy, the energy ejected by supernova explosions is radiated and does not heat up the ISM.

(ii) The present iron abundance of the hot ISM can be less than $1Z_{\odot}$ and consistent with the *ASCA* observations if the abundance of the mass-loss gas has wide distribution. In this case, the mass-loss gas with higher abundance also drops out in addition to the shells of the supernova remnant. This effect makes the observed average abundance of the ISM lower. Although our model may be too simple to give quantitative predictions, we believe this is a hint of solving the low abundance problem of elliptical galaxies.

(iii) If the model spectra are fitted by one thermal spectrum model, the resultant abundance is well below $1Z_{\odot}$, although the fits suffer from significant positive residuals above ~ 2 keV. When they are fitted by two thermal spectrum models, χ^2 is significantly reduced and the derived abundances are also subsolar.

We thank N. Gouda, H. Kodama, S. Ikeuchi, N. Arimoto, H. Sato, J. Yokoyamka, Y. Yamada, R. Nishi, and T. Shigeyama for useful discussion and comments. Y. Fujita thanks K. Koyama for the use of a computer. We are also grateful to K. Matsushita and H. Matsumoto for providing *ASCA* data. This work was supported in part by the JSPS Research Fellowship for Young Scientists.

REFERENCES

Arimoto, N., & Yoshii, Y. 1987, A&A, 173, 23

Awaki, H., Mushotzky, R., Tsuru, T., Fabian, A. C., Fukazawa, Y., Loewenstein, M., Makishima, K., Matsumoto, H., Matsushita, K., Mihara, T., Ohashi, T., Ricker, G. R., Serlemitsos, P. J., Tsusaka, Y., & Yamazaki, T. 1994, PASJ, 46, L65

Binney, J., & Tremaine, S. 1987, in Galactic Dynamics (Princeton : Princeton Univ. Press)

Ciotti, L., D'Ercole, A., Pellegrini, S., & Renzini, A. 1991, ApJ, 376, 380

Cowie, L. L., Fabian, A. C., & Nulsen, P. E. J. 1980, MNRAS, 191, 399

David, L. P., Forman, W., & Jones, C. 1990, ApJ, 359, 29

David, L. P., Forman, W., & Jones, C. 1991, ApJ, 380, 39

Fukumoto, J., & Ikeuchi, S. 1996, PASJ, 48, 1

Ikeuchi, S. 1977, Prog. Theor. Phys., 58, 1742

Kaastra, J.S. 1992, An X-Ray Spectral Code for Optically Thin Plasmas (Internal SRON-Leiden Report, updated version 2.0)

Kim, D. -W., & Fabbiano, G. 1995, ApJ, 441, 182

Köppen, J., & Arimoto, N. 1991, A&AS, 87, 109

Larson, R. B. 1974, MNRAS, 166, 585

Matsushita, K., Makishima, K., Awaki, H., Canizares, C. R., Fabian, A. C., Fukazawa, Y., Loewenstein, M., Matsumoto, H., Mihara, T., Mushotzky, R. F., Ohashi, T., Ricker, G. R., Serlemitsos, P. J., Tsuru, T., Tsusaka, Y., & Yamazaki, T. 1994, ApJ, 436, L41

Mathews, W. G. 1990, ApJ, 354, 468

Matteucci, F., & Gibson, B. K. 1995, A&A, 304, 11

Matteucci, F., & Tornambé, A. 1987, A&A, 185, 51

Mewe, R., Gronenschild, E.H.B.M., & van den Oord, G.H.J. 1985, A&AS, 62, 197

Mewe, R., Lemen, J.R., & van den Oord, G.H.J. 1986, A&AS, 65, 511

Mihara, K., & Takahara, F. 1994, PASJ, 46, 447

Renzini, A., Ciotti, L., D'Ercole, A., & Pellegrini, S. 1993, ApJ, 419, 52

Spitzer, L. 1978, in Physical Processes in the Interstellare Medium (New York : Wiley)

Figure Captions

Fig. 1.— The evolution of (a) radius (b) gas mass and (c) abundance for models A1 - A3.

Fig. 2.— The evolution of (a) radius (b) gas mass and (c) abundance for models B1 - B3.

Fig. 3.— The evolution of (a) radius (b) gas mass and (c) abundance for models A1, A4 and A5.

Fig. 4.— The evolution of (a) radius (b) gas mass and (c) abundance for models B1, B4 and B5.

Fig. 5.— Simulated X-ray spectra observed with the *ASCA* SIS. The line shows the best fitting (one Meka plasma + absorption column density). (a) Model A1 (b) Model A2 (c) Model B4

Fig. 6.— Simulated X-ray spectra observed with the *ASCA* SIS. The line shows the best fitting (two Meka plasma + absorption column density). (a) Model A1 (b) Model A2 (c) Model B4

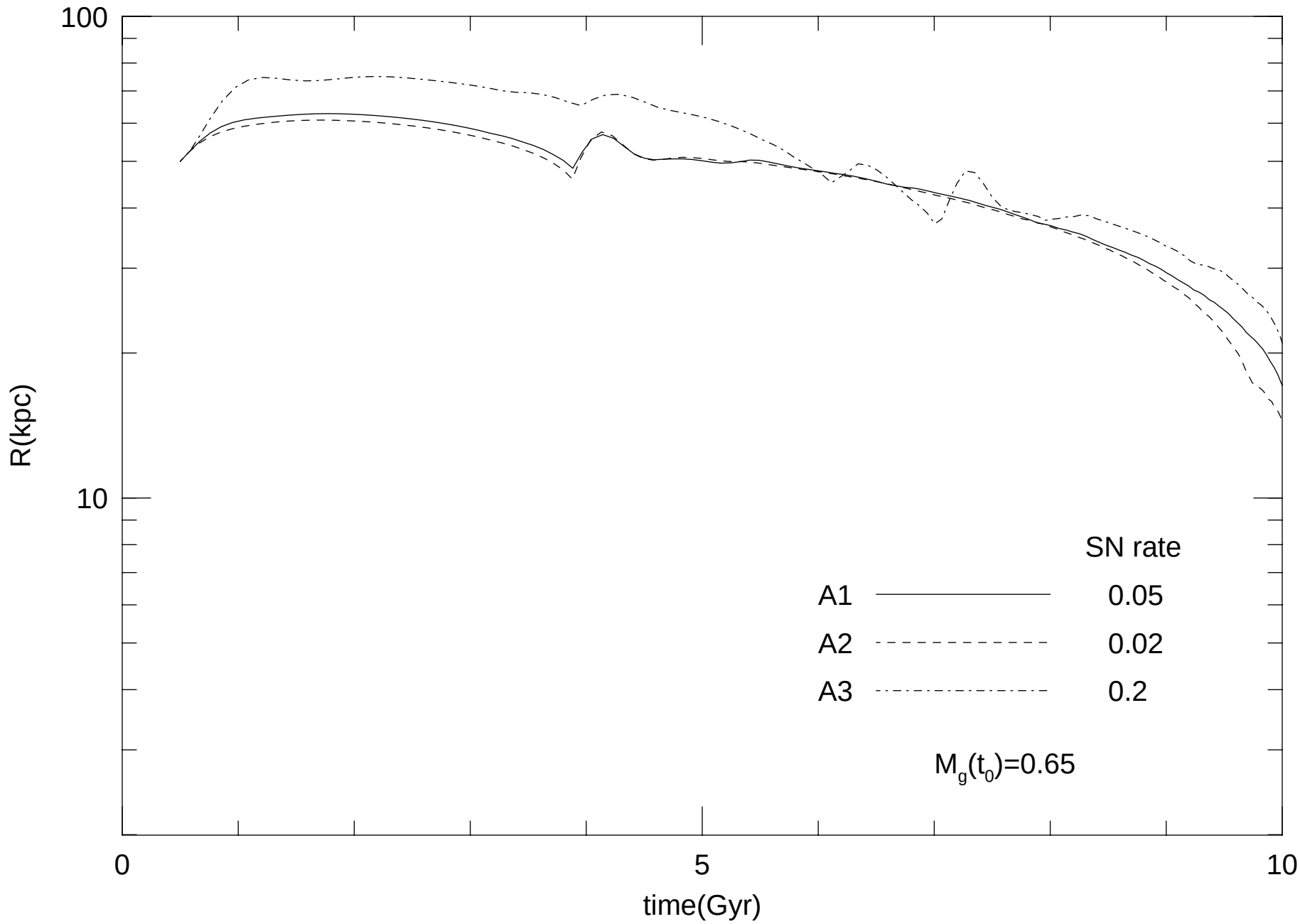
100
10
R(kpc)
0
5
10
time(Gyr)
SN rate
A1
0.05
A2
0.02
A3
0.2
$M_g(t_0)=0.65$

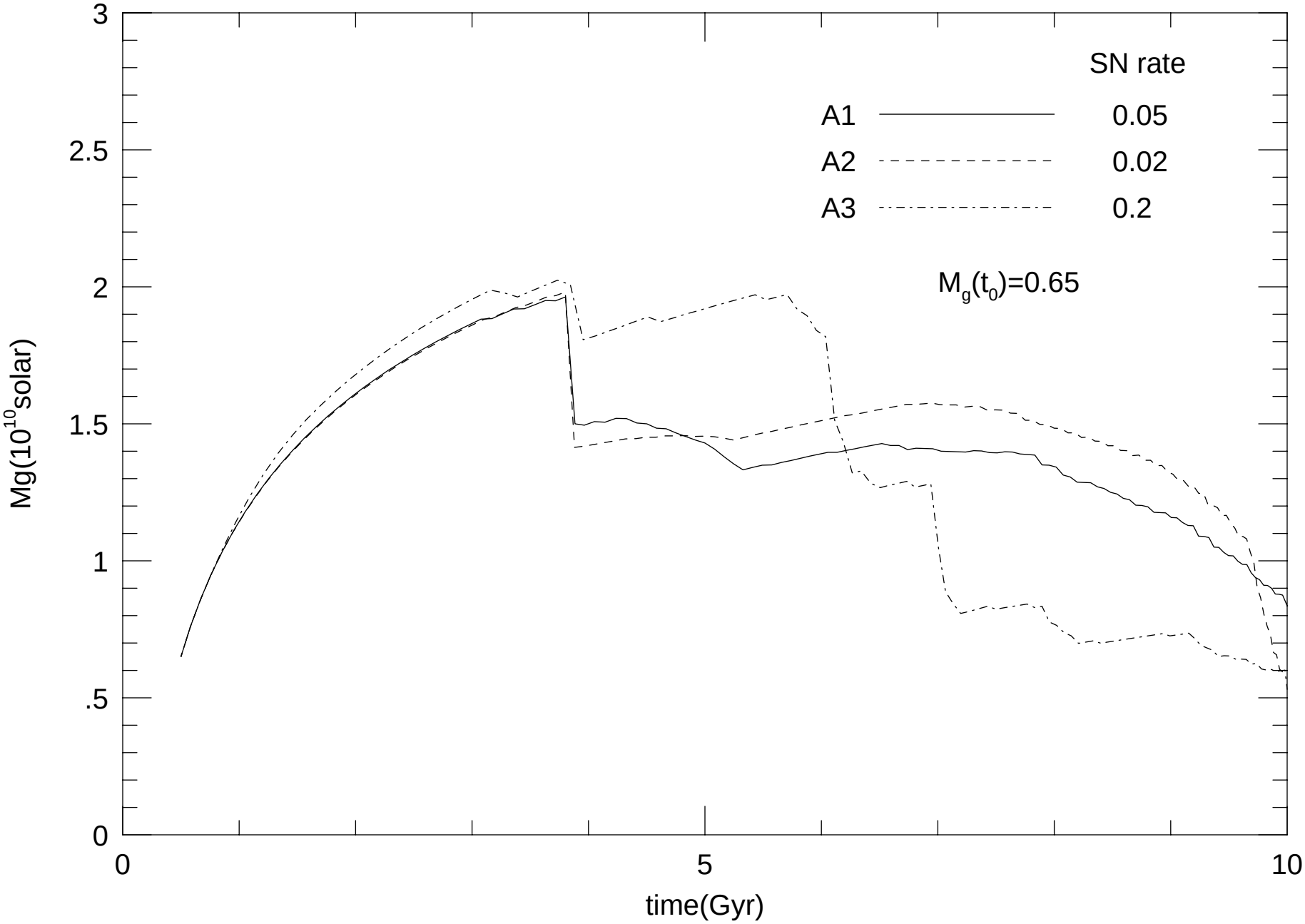
SN rate
A1 0.05
A2 0.02
A3 0.2
$M_g(t_0)$=0.65
Mg(10^{10}solar)
time(Gyr)
0
.5
1
1.5
2
2.5
3
0
5
10

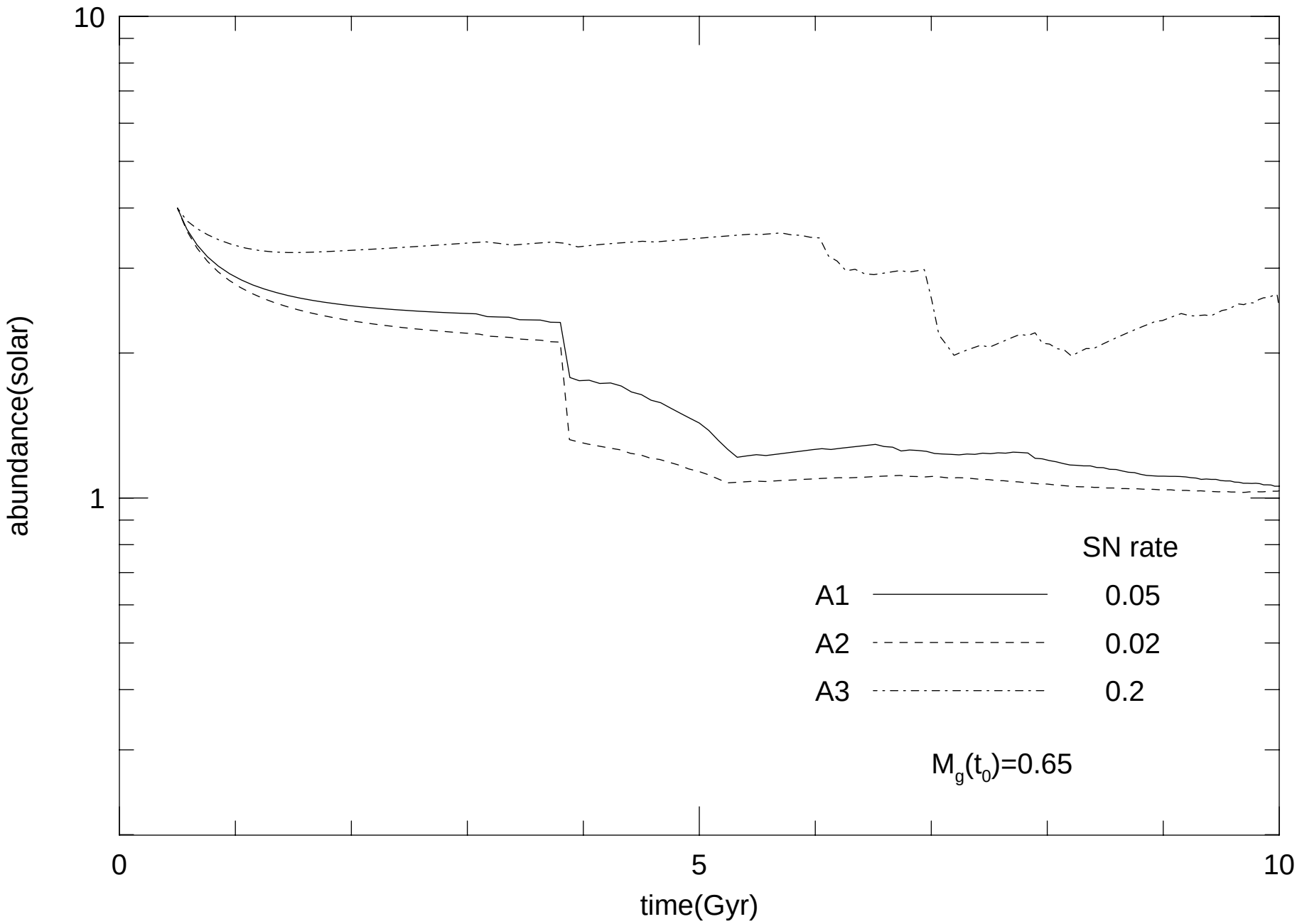
10
1
abundance(solar)
0
5
10
time(Gyr)
SN rate
A1
0.05
A2
0.02
A3
0.2
$M_g(t_0)=0.65$

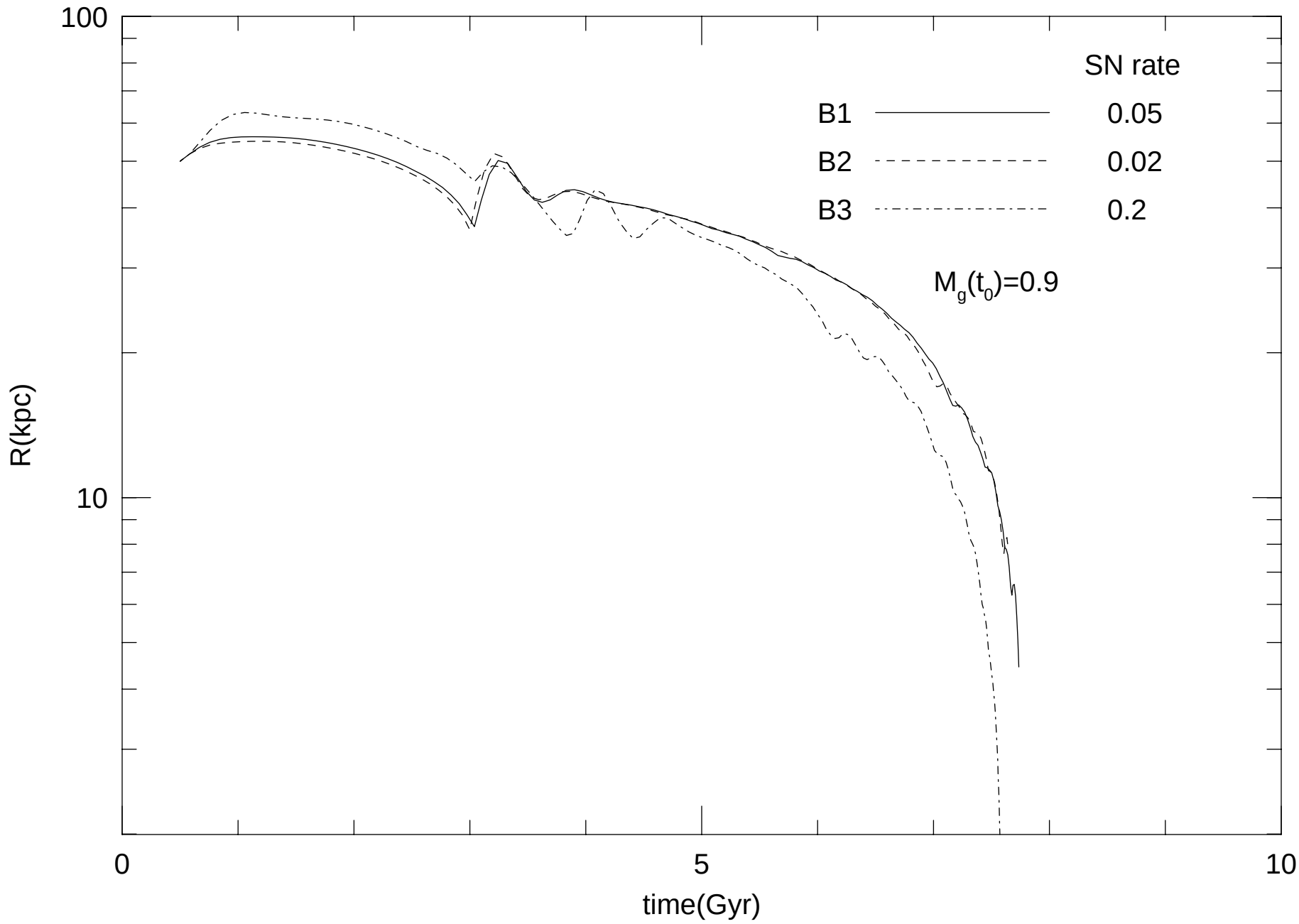
100
10
R(kpc)
0
5
10
time(Gyr)
SN rate
B1
0.05
B2
0.02
B3
0.2
$M_g(t_0)=0.9$

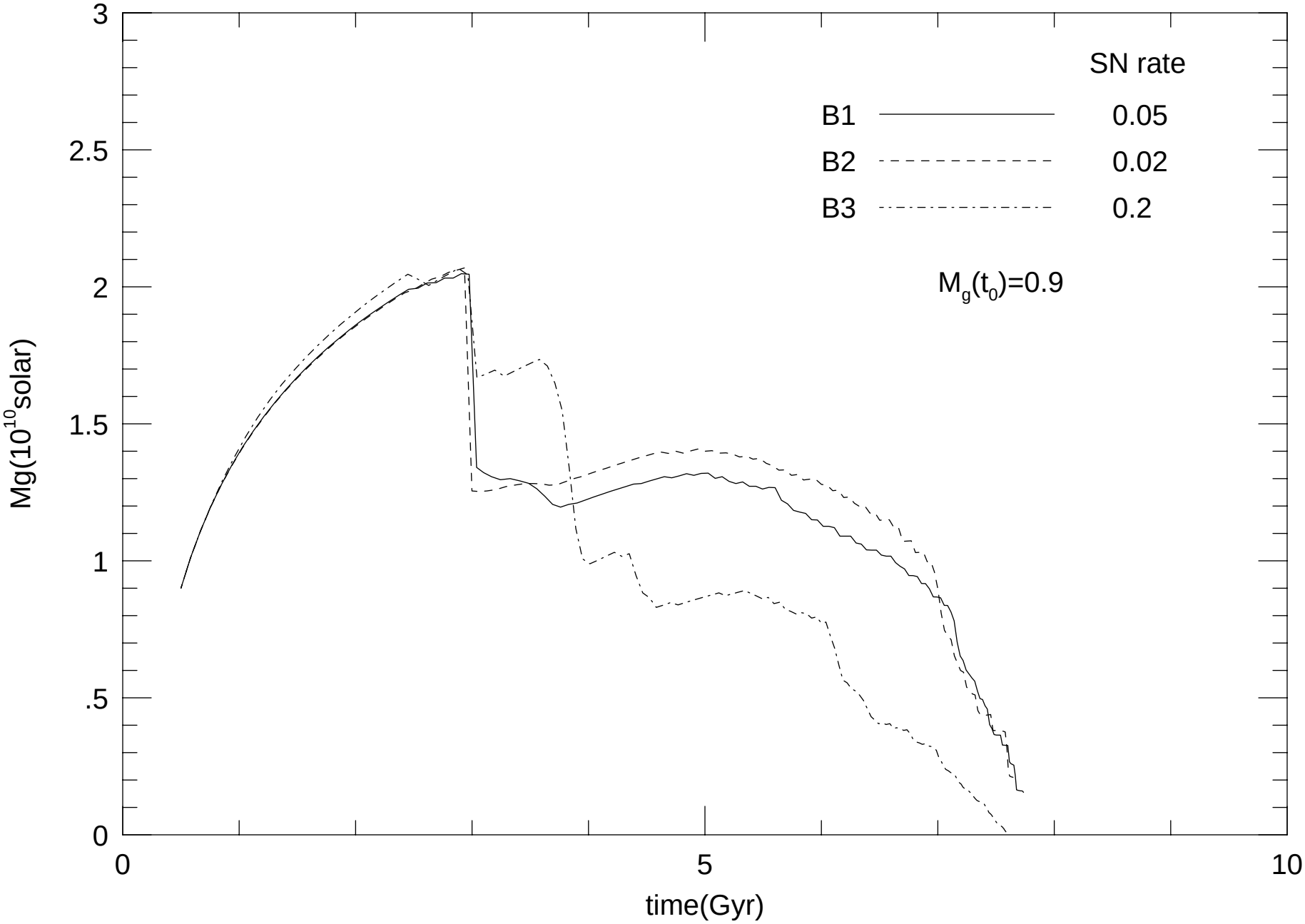
SN rate
B1 0.05
B2 0.02
B3 0.2
$M_g(t_0)=0.9$
Mg(10^{10}solar)
time(Gyr)
0
.5
1
1.5
2
2.5
3
0
5
10

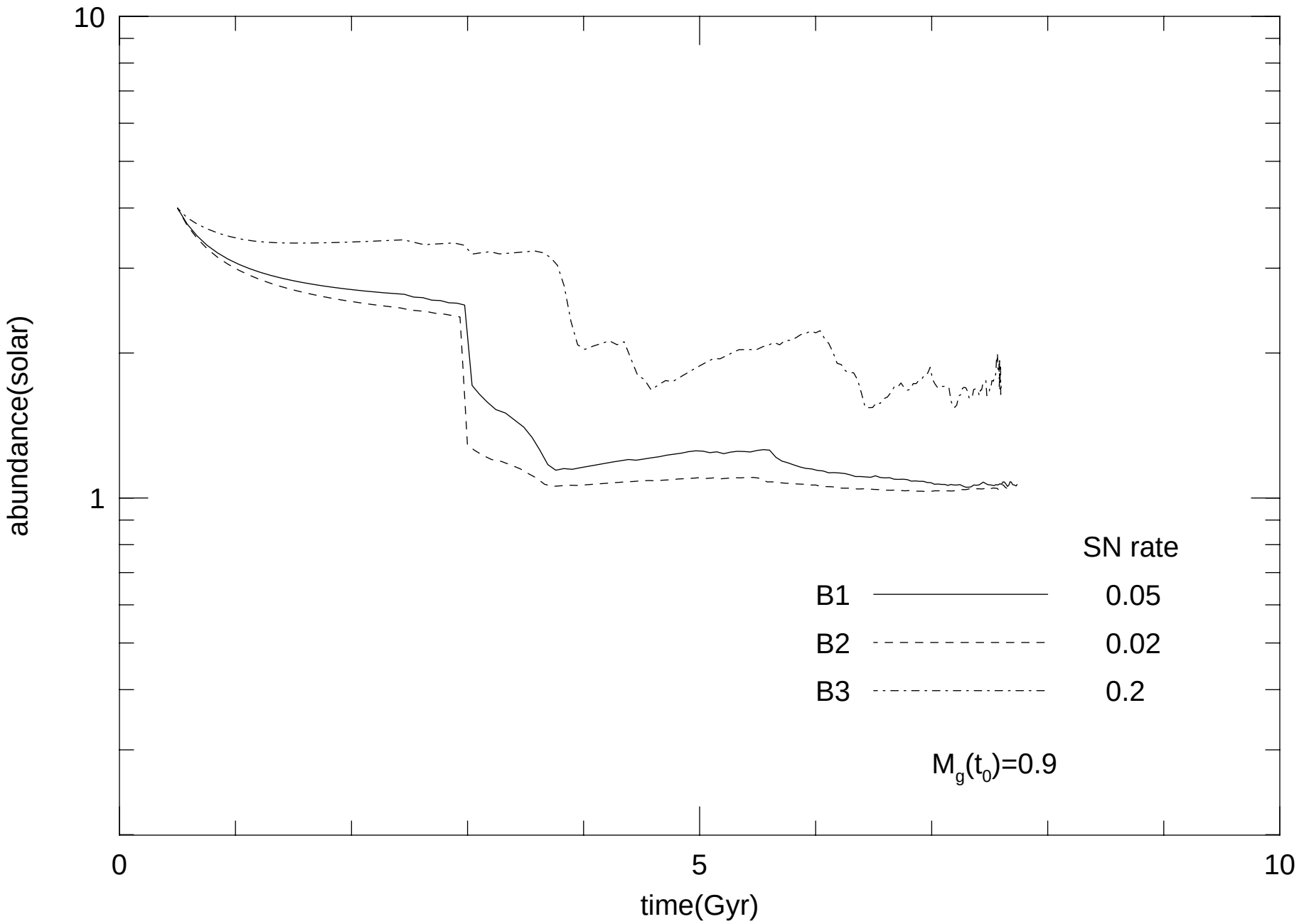
10
1
abundance(solar)
0
5
10
time(Gyr)
SN rate
B1
0.05
B2
0.02
B3
0.2
$M_g(t_0)=0.9$

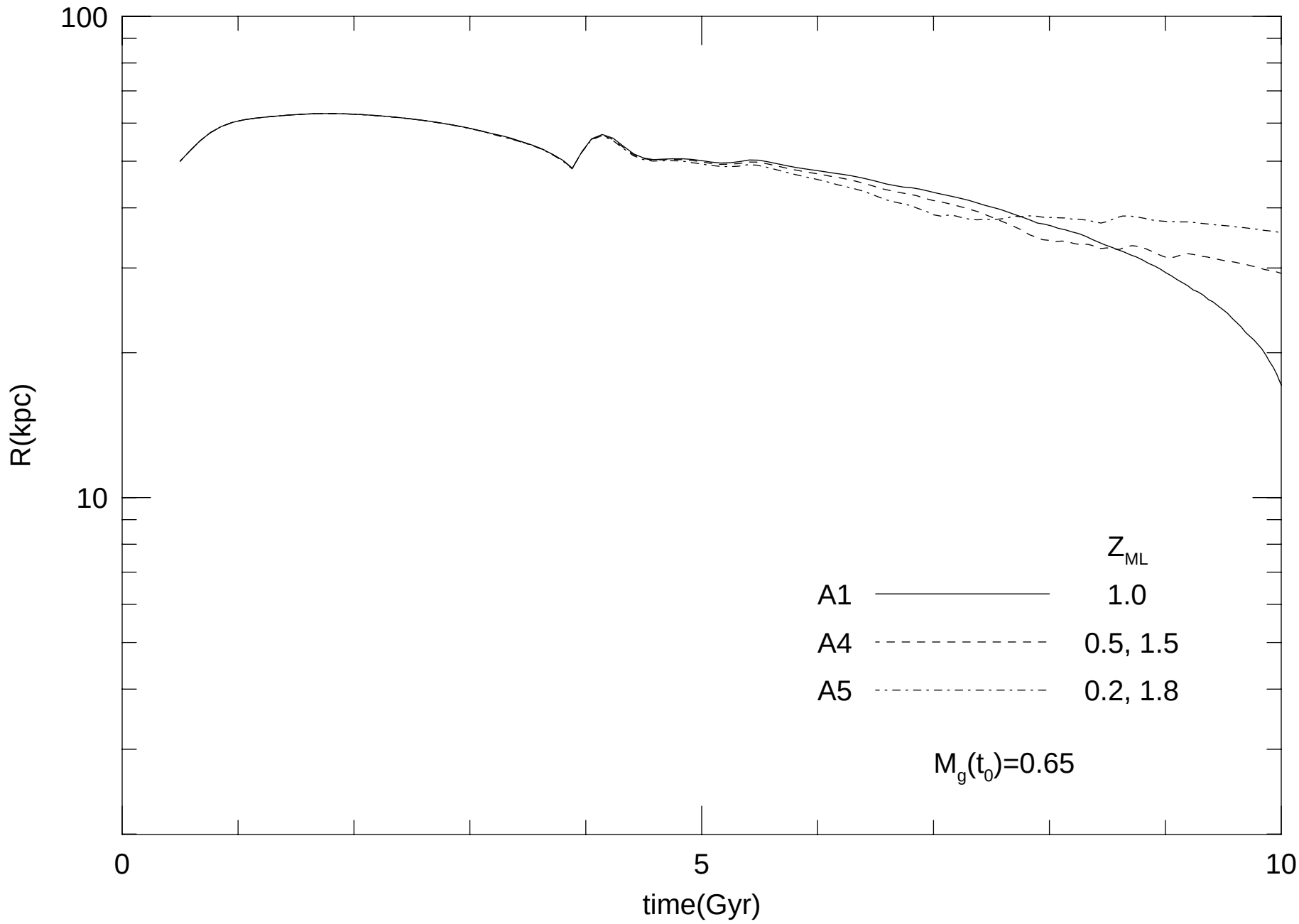
100
10
R(kpc)
0
5
10
time(Gyr)
Z_{ML}
A1
1.0
A4
0.5, 1.5
A5
0.2, 1.8
$M_g(t_0)$=0.65

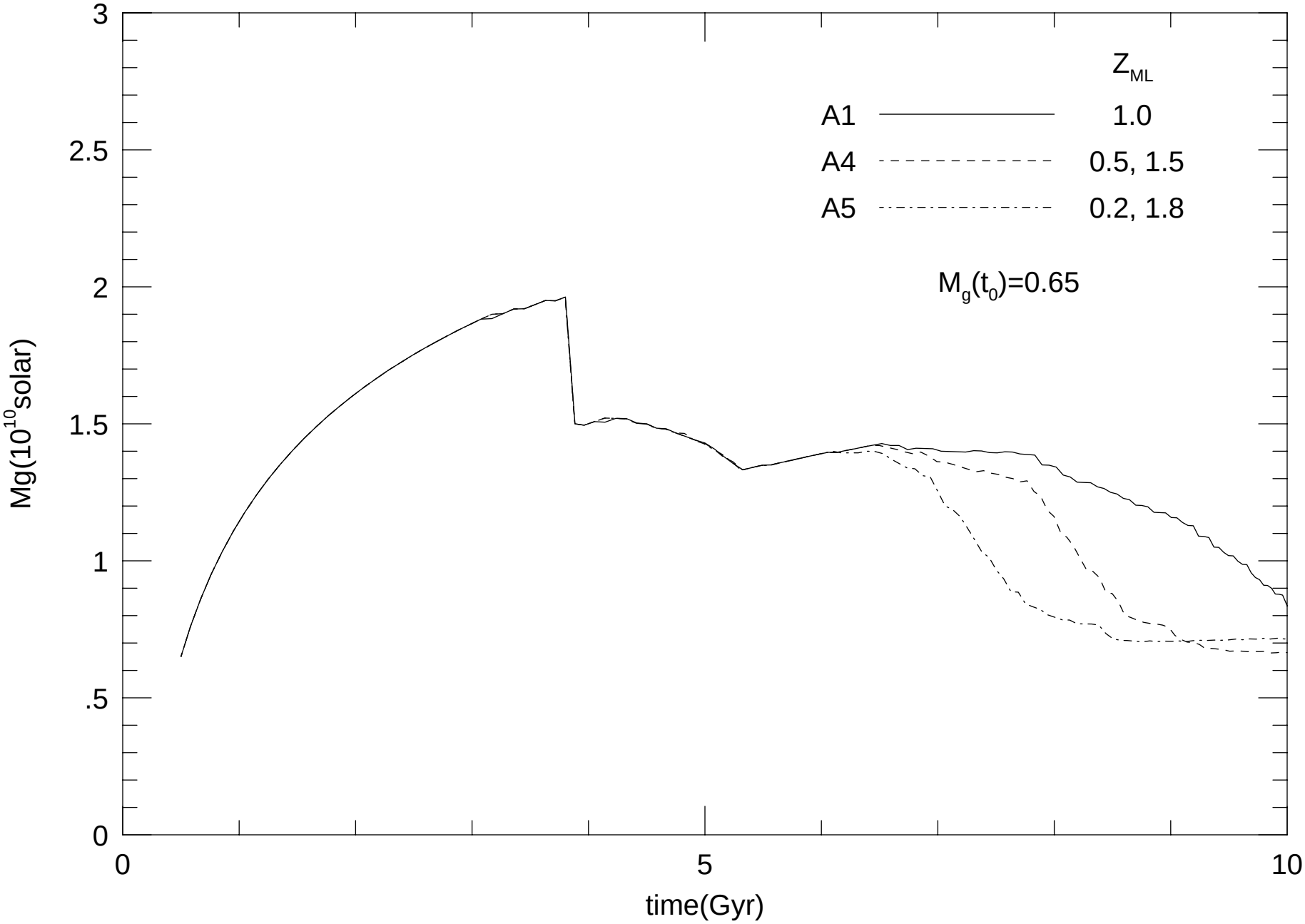
3
2.5
2
1.5
1
.5
0
0
5
10
Mg(10^10solar)
time(Gyr)
Z_ML
A1
1.0
A4
0.5, 1.5
A5
0.2, 1.8
M_g(t_0)=0.65

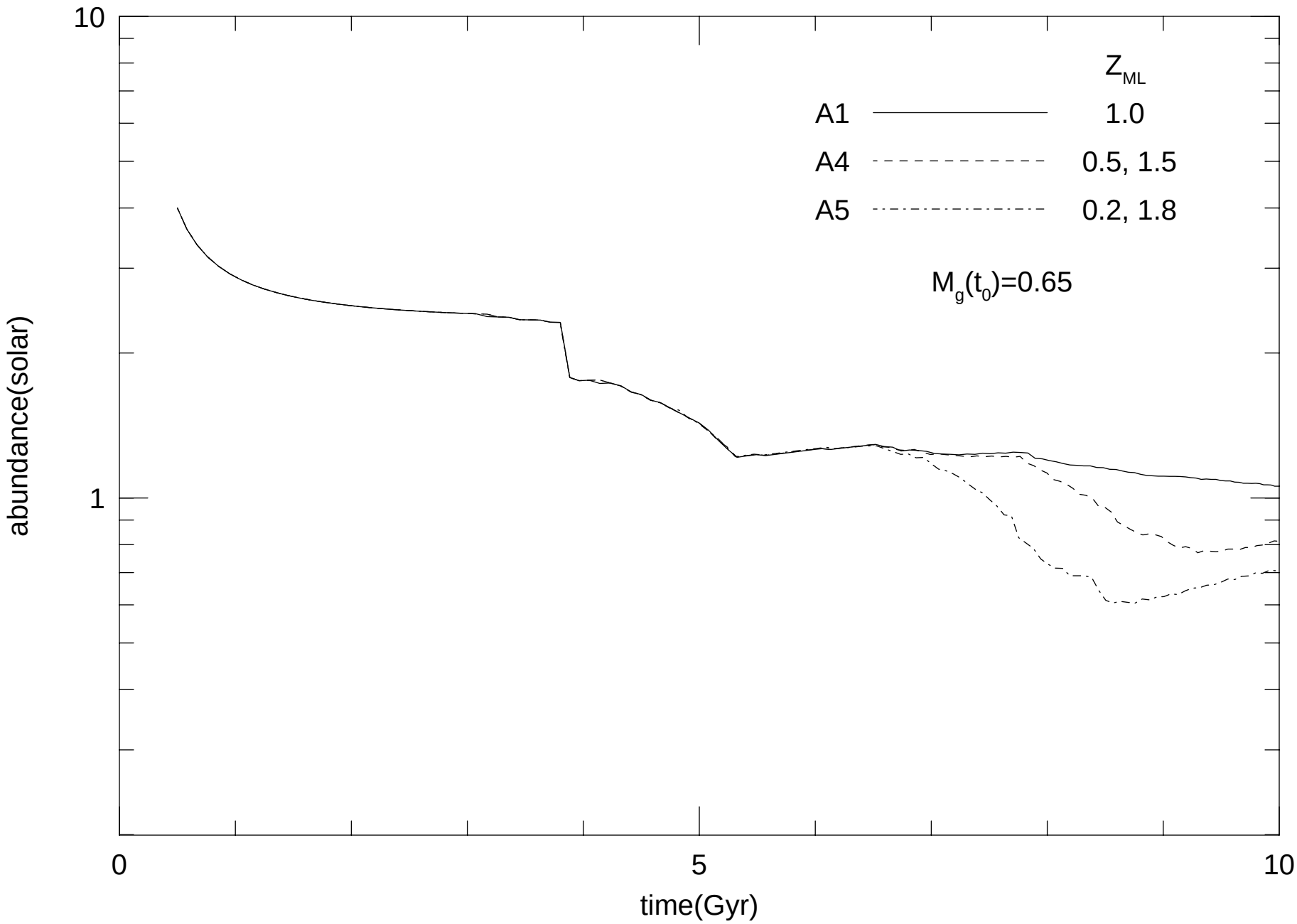
10
1
0
5
10
abundance(solar)
time(Gyr)
Z_{ML}
A1
1.0
A4
0.5, 1.5
A5
0.2, 1.8
$M_g(t_0)$=0.65

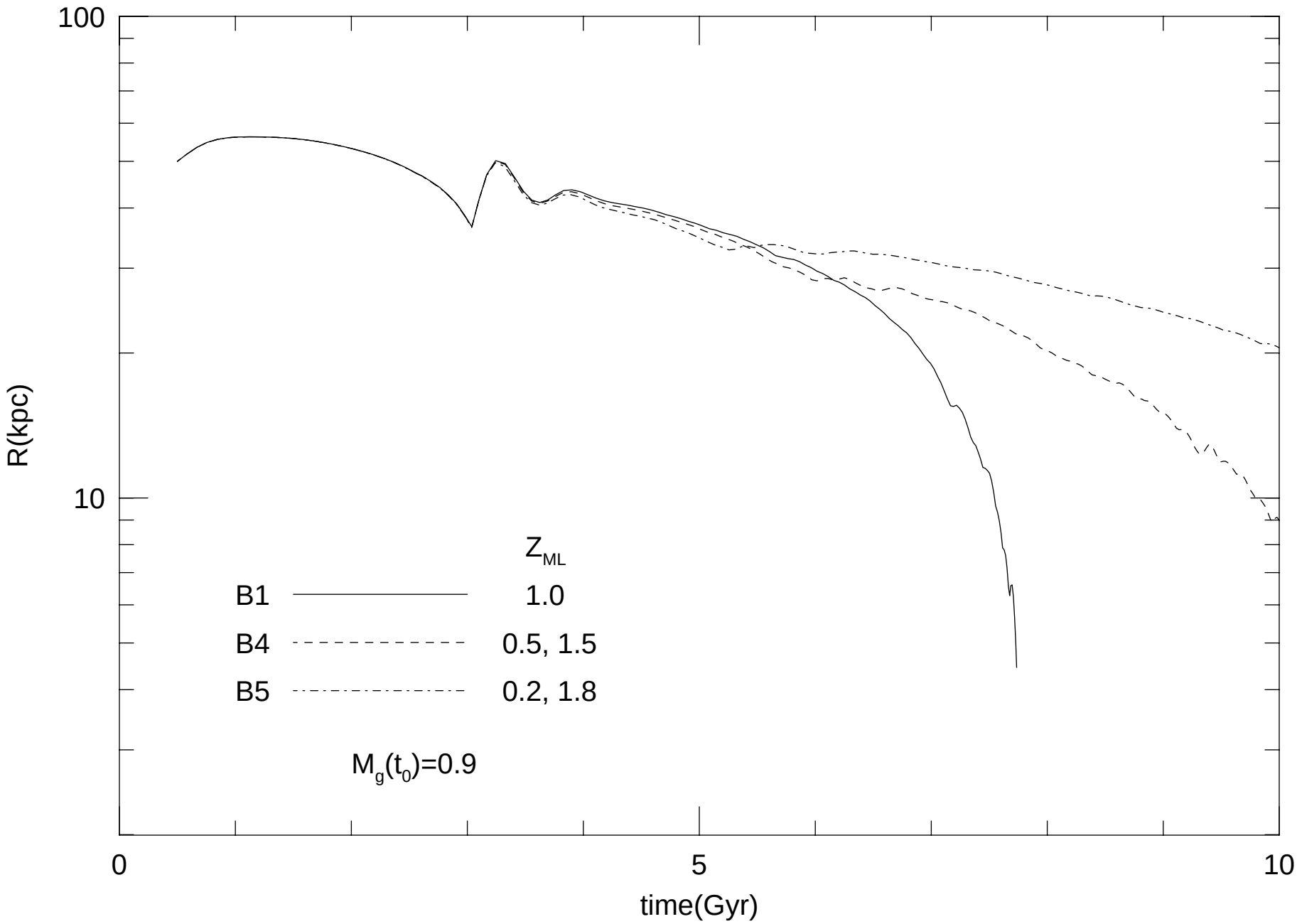
100
10
R(kpc)
0
5
10
time(Gyr)
Z_{ML}
B1
1.0
B4
0.5, 1.5
B5
0.2, 1.8
$M_g(t_0)$=0.9

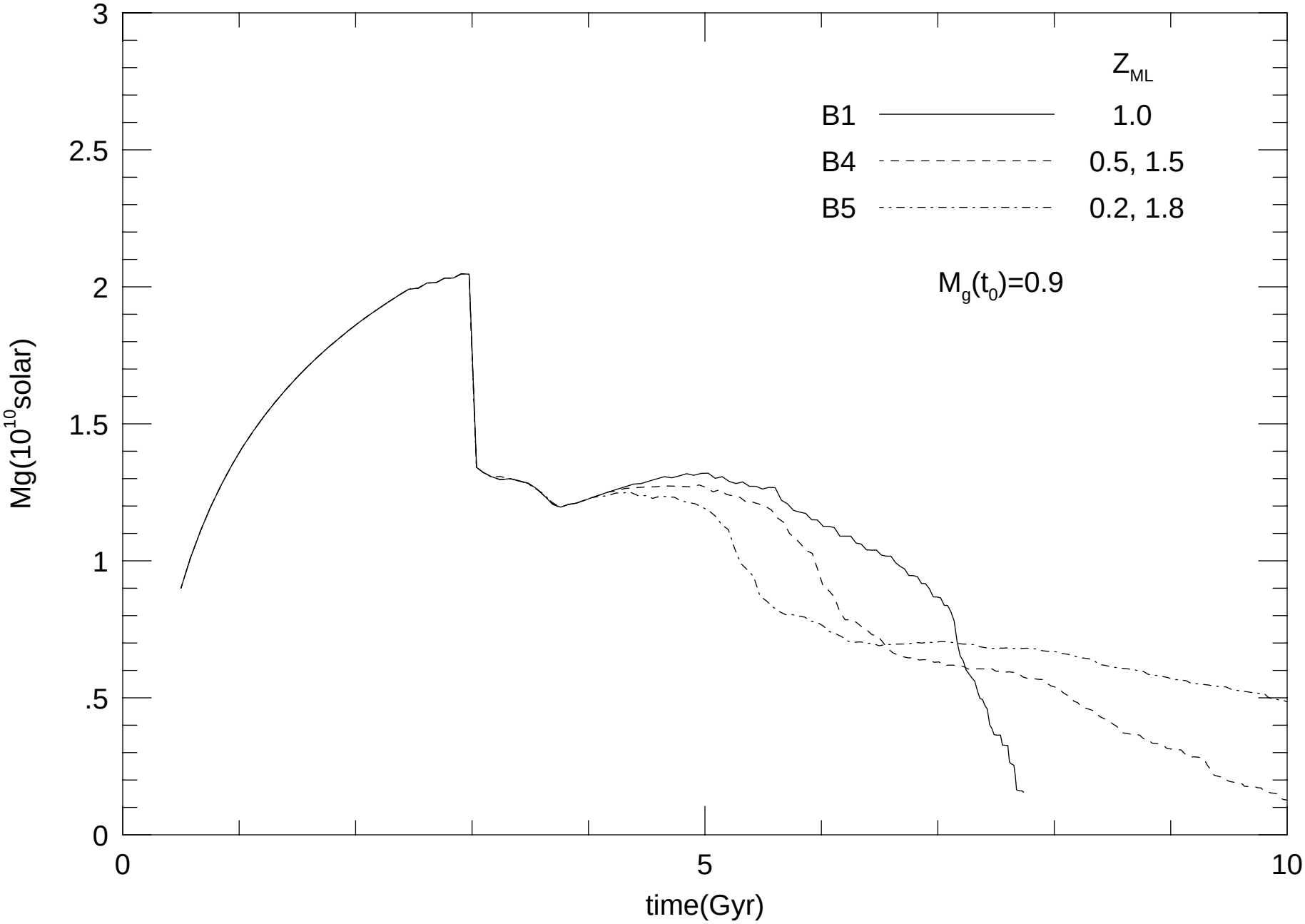
3
2.5
2
1.5
1
.5
0
0
5
10
Mg(10^10solar)
time(Gyr)
Z_ML
B1
1.0
B4
0.5, 1.5
B5
0.2, 1.8
M_g(t_0)=0.9

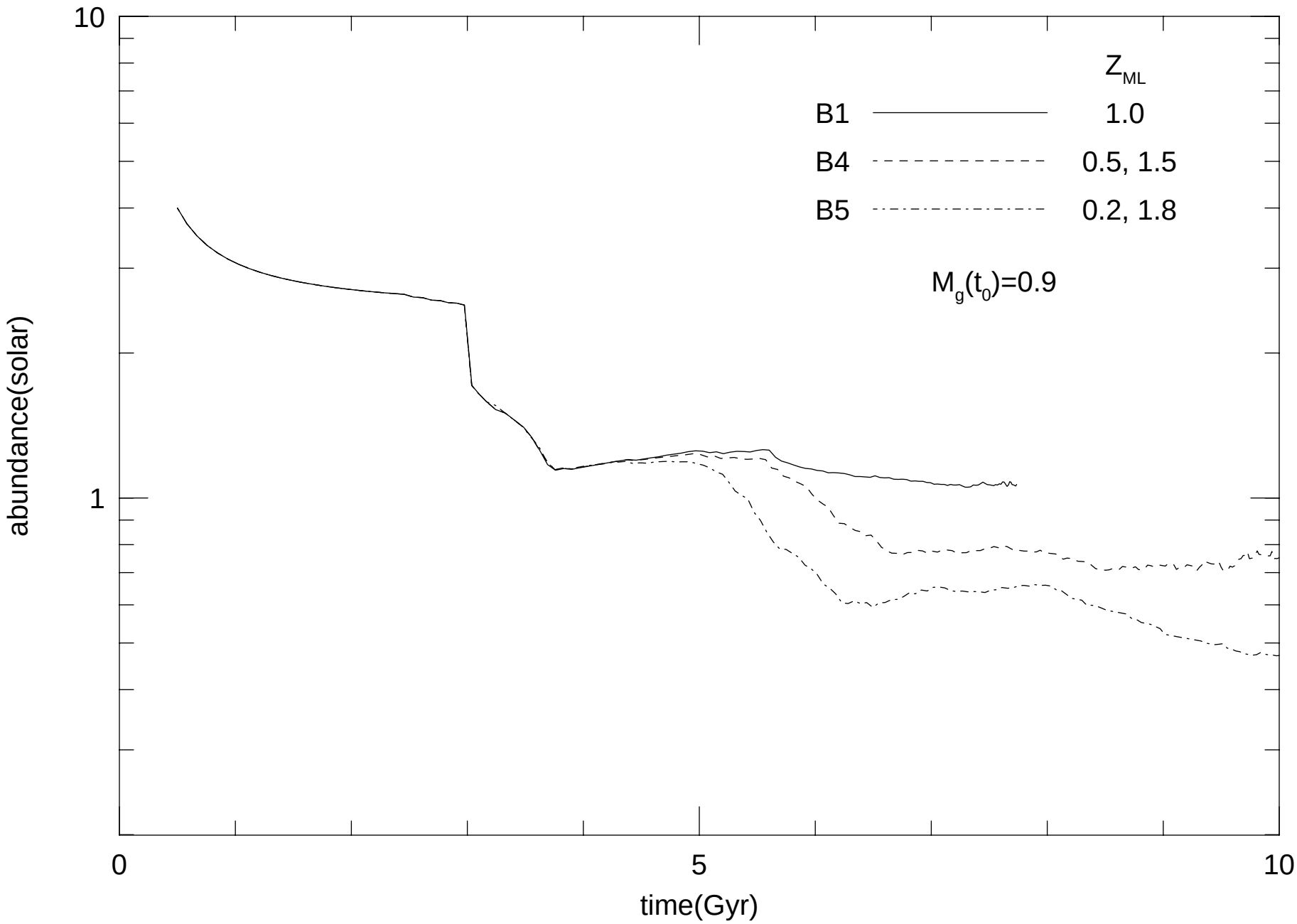
10
1
0
5
10
abundance(solar)
time(Gyr)
Z_{ML}
B1
1.0
B4
0.5, 1.5
B5
0.2, 1.8
$M_g(t_0)$=0.9

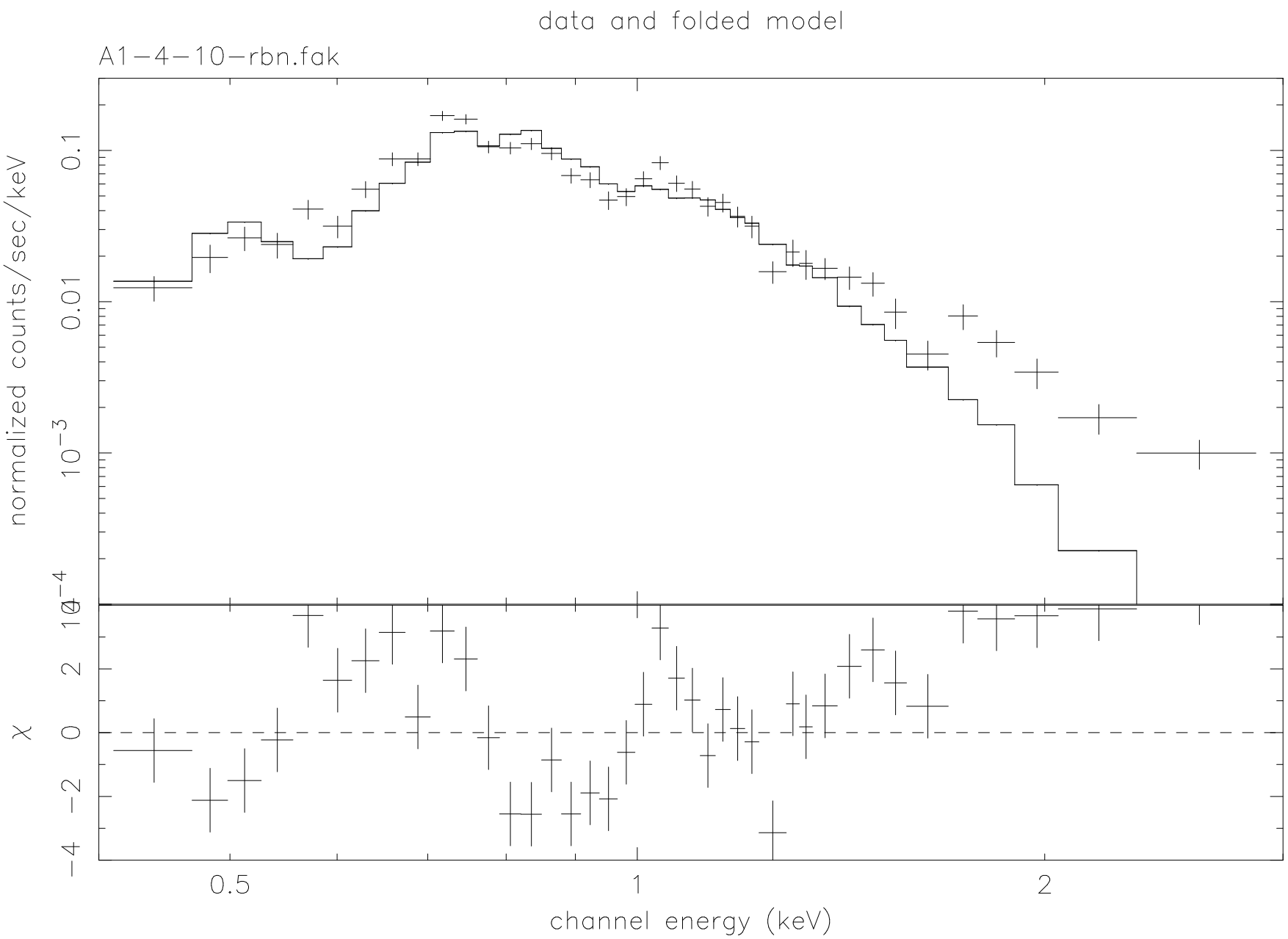
data and folded model
A1−4−10−rbn.fak
normalized counts/sec/keV
0.1
0.01
10^{-3}
10^{-4}
χ
4
2
0
−2
−4
0.5
1
2
channel energy (keV)

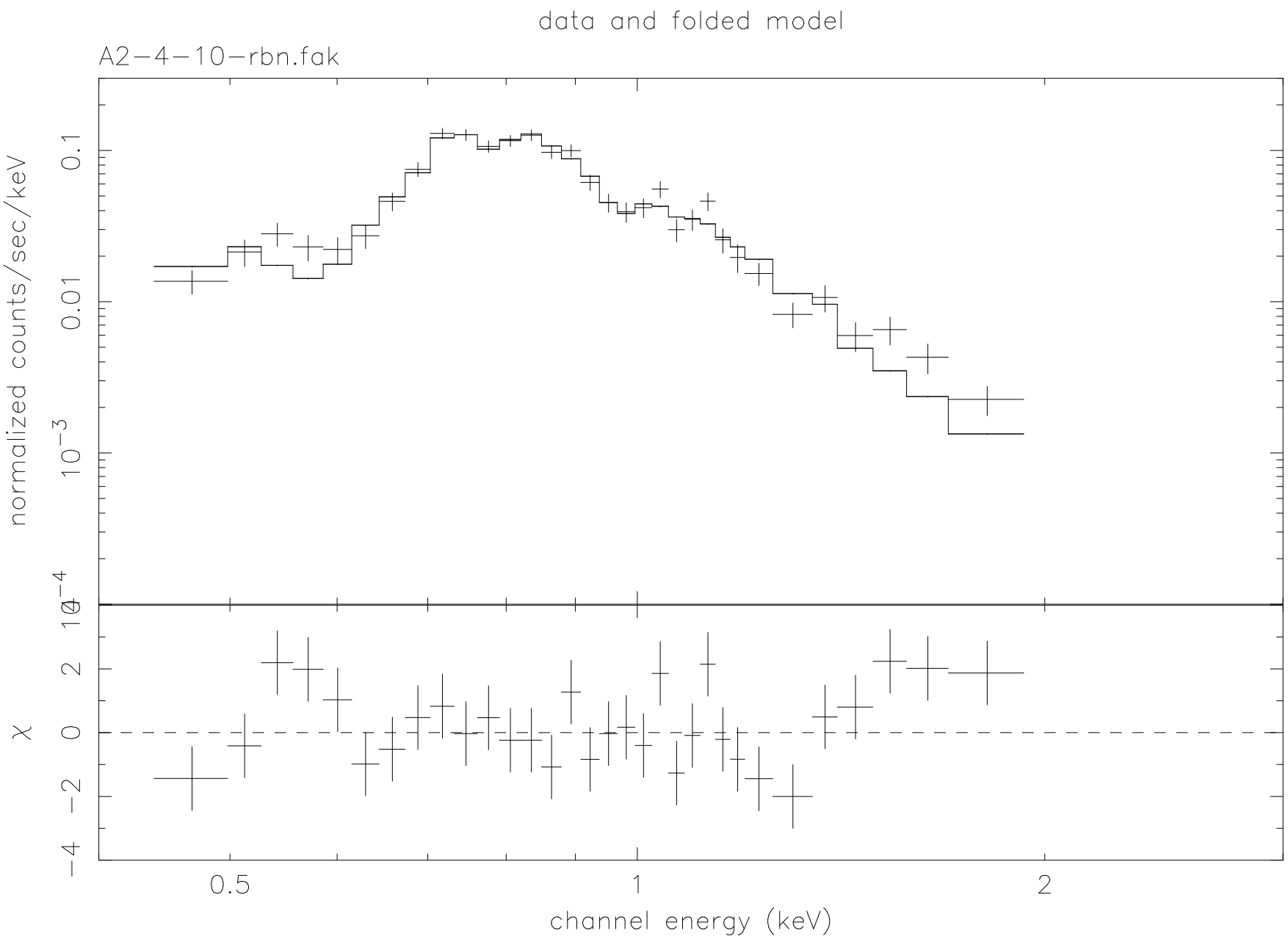
data and folded model
A2−4−10−rbn.fak
normalized counts/sec/keV
0.1
0.01
10^{-3}
10^{-4}
χ
4
2
0
−2
−4
0.5
1
2
channel energy (keV)

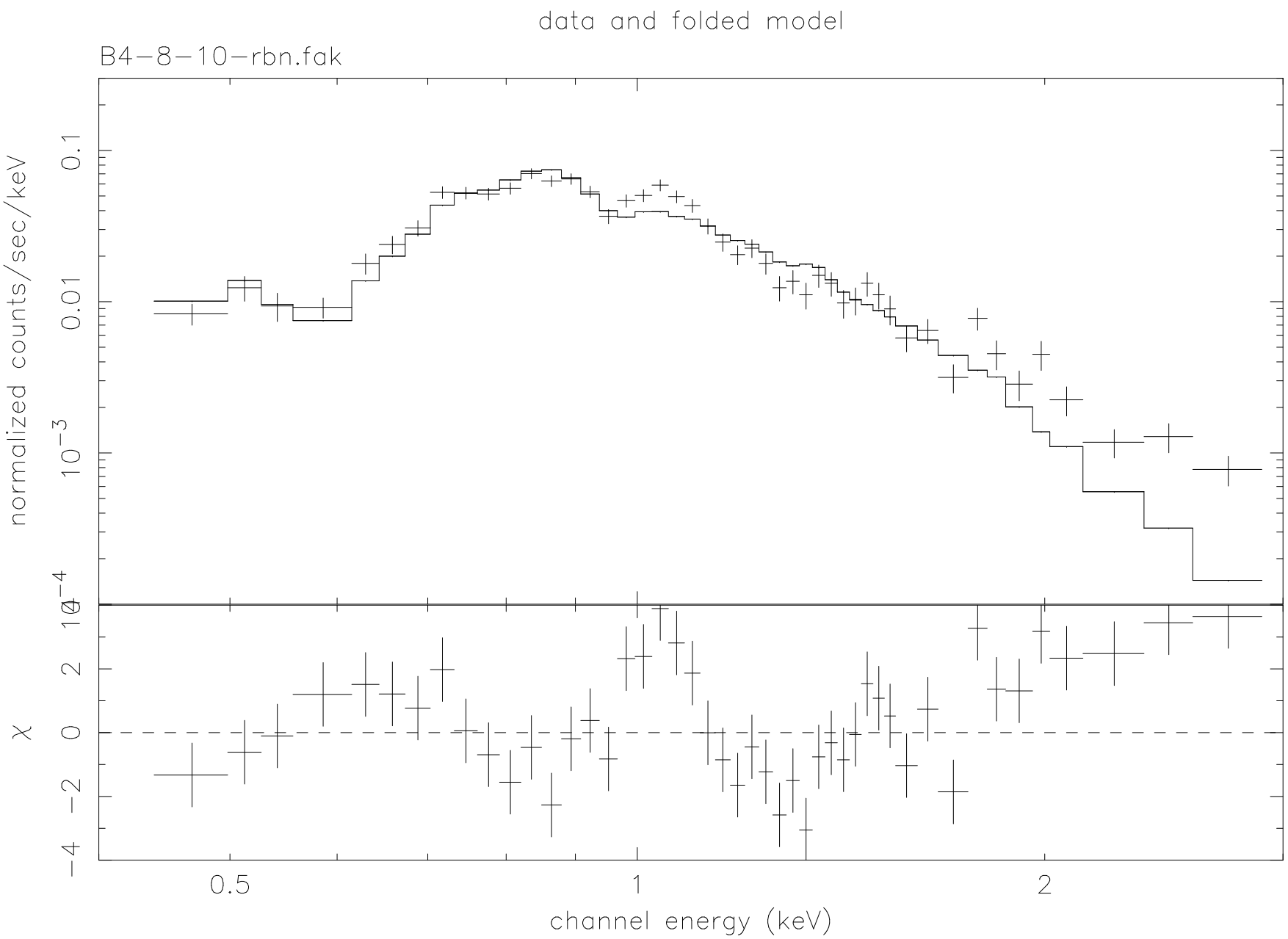
data and folded model
B4−8−10−rbn.fak
normalized counts/sec/keV
0.1
0.01
10^{-3}
10^{-4}
χ
4
2
0
−2
−4
0.5
1
2
channel energy (keV)

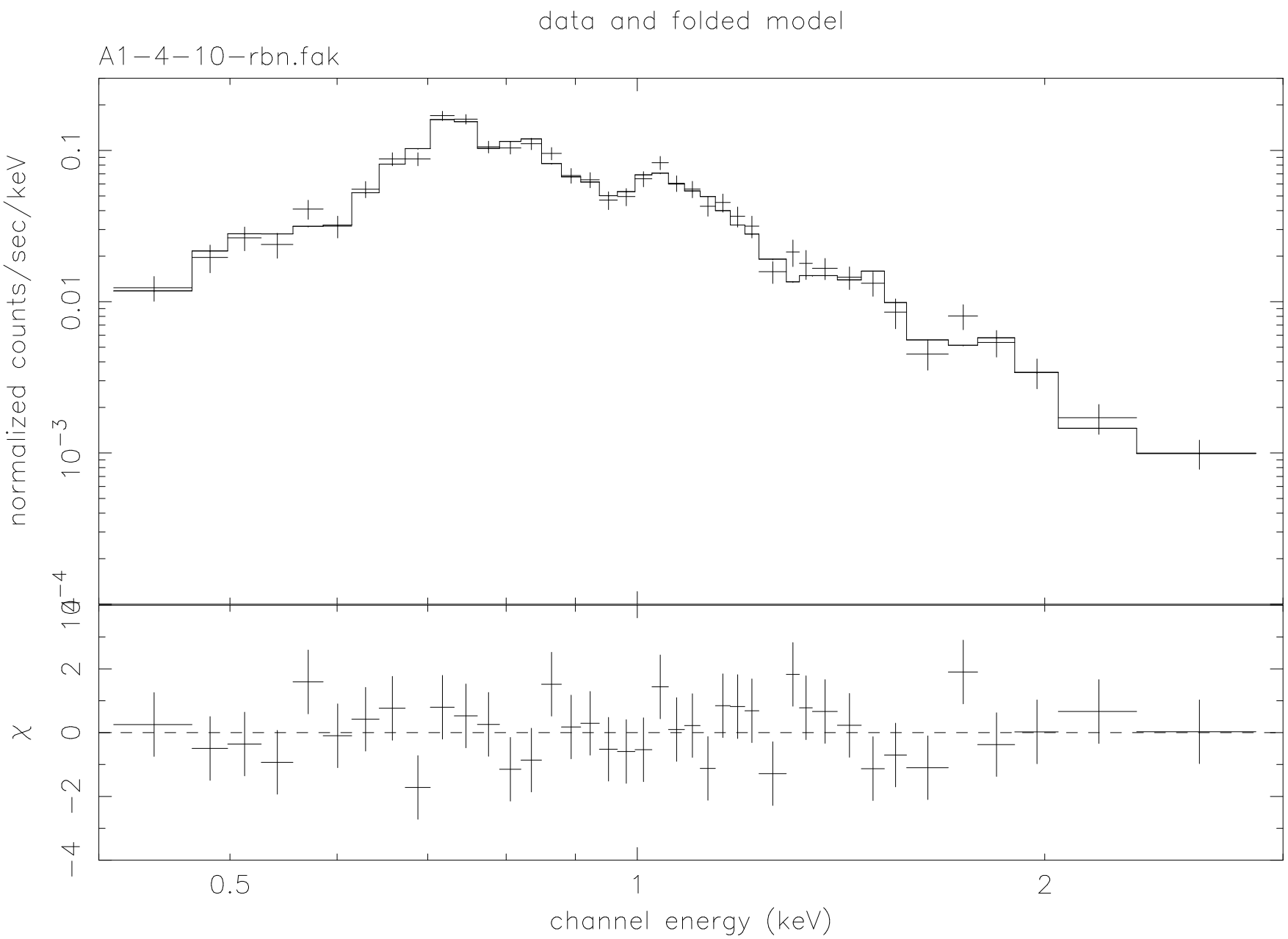
data and folded model
A1−4−10−rbn.fak
normalized counts/sec/keV
0.1
0.01
10^{-3}
10^{-4}
χ
2
0
−2
−4
0.5
1
2
channel energy (keV)

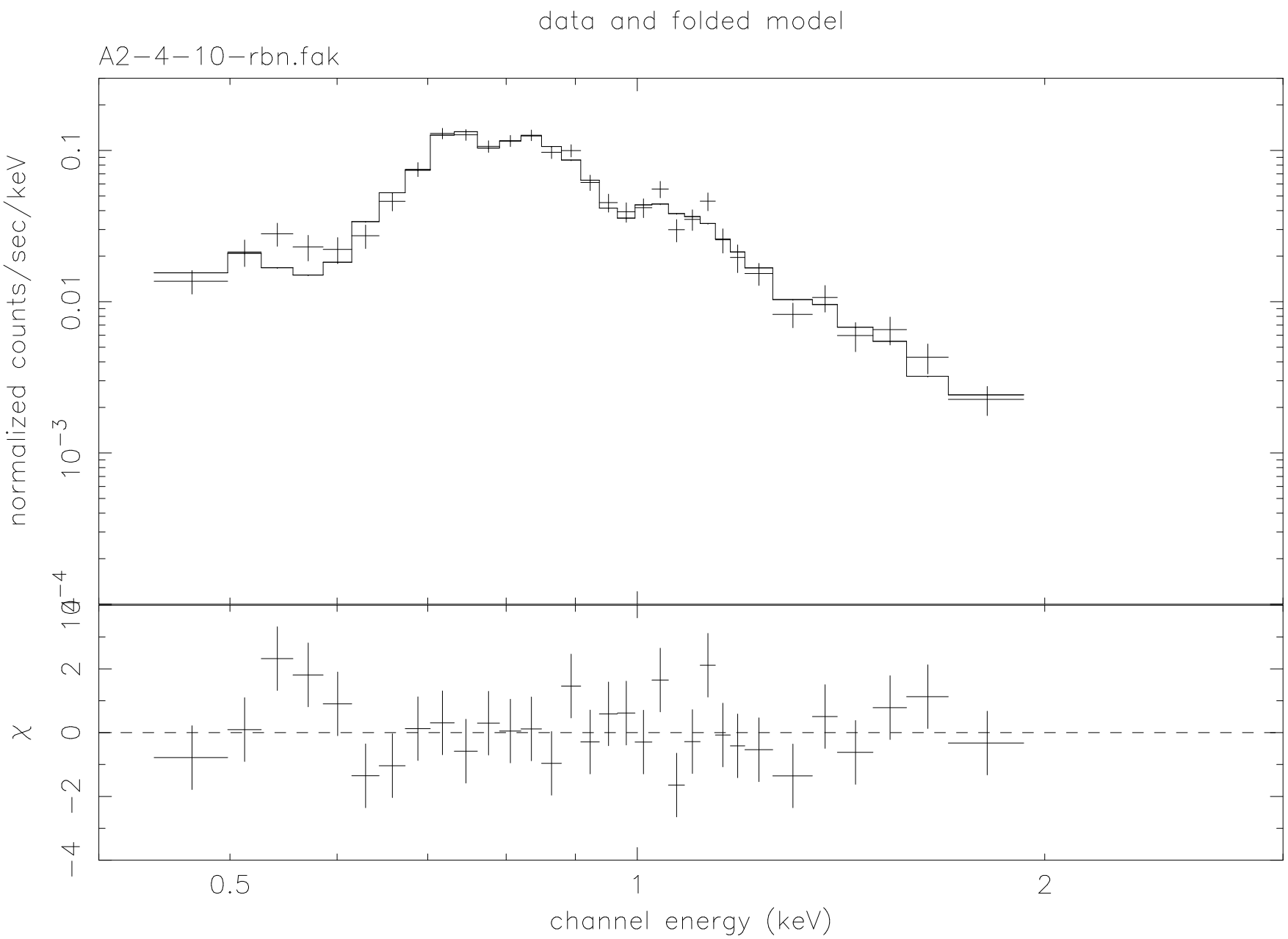
data and folded model
A2−4−10−rbn.fak
normalized counts/sec/keV
0.1
0.01
10^{-3}
10^{-4}
χ
4
2
0
−2
−4
0.5
1
2
channel energy (keV)

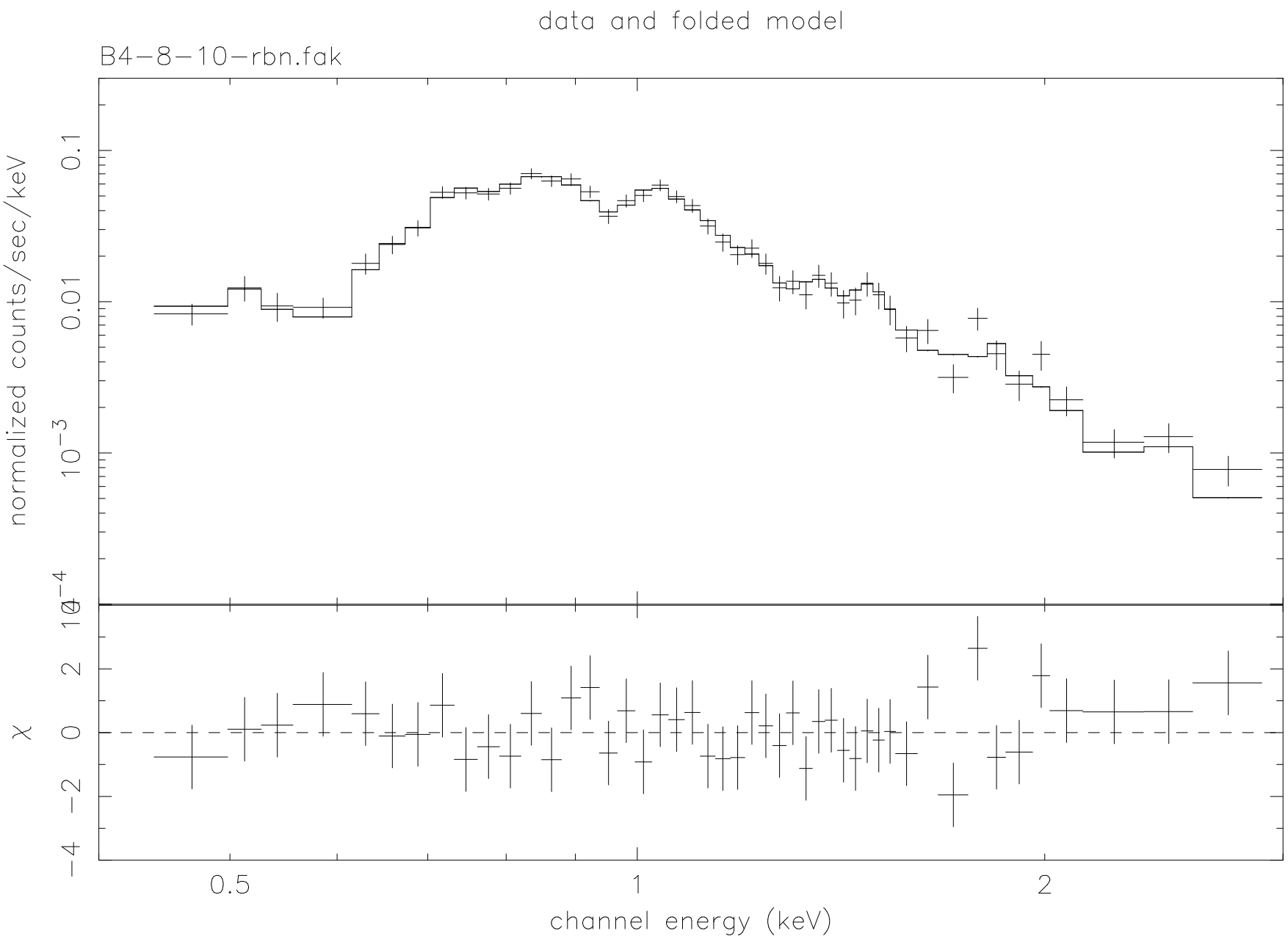
data and folded model
B4−8−10−rbn.fak
normalized counts/sec/keV
0.1
0.01
10^{-3}
10^{-4}
χ
2
0
−2
−4
0.5
1
2
channel energy (keV)

TABLE 1

PARAMETERS OF MODELS

Model	$M_{\rm g}(t_0)$ ($10^{10}{\rm M}_\odot$)	SN rate (SNu)	$Z_{\rm ML}$ ($Z_\odot$)	n	$N_{\rm ML,H}$	$N_{\rm ML,L}$	$N_{\rm sh}$	$N_{\rm cav}$
A1	0.65	0.05	1.0	133	91	91	10	133
A2	0.65	0.02	1.0	138	33	33	7	138
A3	0.65	0.2	1.0	117	107	107	23	117
A4	0.65	0.05	1.5,0.5	128	31	126	25	128
A5	0.65	0.05	1.8,0.2	124	37	124	33	124
B1	0.9	0.05	1.0	147	...	...	...	...
B2	0.9	0.02	1.0	136	...	...	...	...
B3	0.9	0.2	1.0	161	...	...	...	...
B4	0.9	0.05	1.5,0.5	213	21	49	12	213
B5	0.9	0.05	1.8,0.2	168	24	153	21	168

TABLE 2
RESULTS OF FITTING

Model	$L_{\rm X}$ (10^{-40}erg s^{-1})	Flux (10^{-12}erg cm^{-2} s^{-1})	Exposure (ks)	Z ($Z_\odot$)	$Z_{\rm fit}$ ($Z_\odot$)	$T_{\rm fit}$ (keV)	$N_{\rm H,fit}$ (10^{21}cm^{-2})	χ^2/dof
A1	24.6	9.1	40	1.1	0.03	0.25	0.26	200/35
					0.65	0.23, 1.0	0.08	32.4/32
A2	13.6	5.1	40	1.0	0.10	0.32	0.11	48.1/27
					0.36	0.33, 1.2	0.00	32.4/24
A3	1.5	0.5	···	2.3	···	···	···	···
A4	0.3	0.1	···	0.8	···	···	···	···
A5	0.1	0.03	···	0.7	···	···	···	···
B1	···	···	···	···	···	···	···	···
B2	···	···	···	···	···	···	···	···
B3	···	···	···	···	···	···	···	···
B4	8.6	3.2	80	0.8	0.04	0.41	0.20	133/42
					0.43	0.40, 1.0	0.02	37.5/39
B5	1.5	0.6	···	0.5	···	···	···	···